# RADIONUCLIDE ANALYSIS OF SOIL SAMPLES TAKEN FROM OUTJO, NAMIBIA.

A MINI THESIS

SUBMITTED IN PARTIAL FULFILMENT

OF THE REQUIREMENTS FOR THE DEGREE OF

MASTER OF SCIENCE IN NUCLEAR SCIENCE

OF

THE UNIVERSITY OF NAMIBIA

BY

LUSINA VENOMUFENU HANGA

201206396

NOVEMBER 2019

Supervisor: Professor J.A. Oyedele (Department of Physics, University of Namibia)

Co-Supervisor: Dr Gotfried Uiseb (Department of Chemistry and Bio-Chemistry, University of Namibia)

## ABSTRACT

Naturally occurring radionuclides such as Uranium ($^{238}U$), Thorium ($^{232}Th$) and Potassium ($^{40}K$), exist in the soil where they continuously disintegrate and emit ionising radiation which could pose health hazards to the inhabitants of a given location if the concentrations of the radionuclides are very high. In this work, the concentrations of the radionuclides $^{238}U$, $^{232}Th$ and $^{40}K$ in the soil samples taken from Outjo have been studied by gamma spectrometry. The town of Outjo was divided into ten geographical areas and five samples were collected across each area. These samples were dried under laboratory temperature, passed through a 2 mm mesh screen and sealed in 500 ml polythene bottles. The samples were analysed using a liquid nitrogen cooled High Purity Germanium (HPGe) detector (by Canberra). The Python Code was used to calculate the activity concentrations of- and Hazard indices due to- the radionuclides $^{238}U$, $^{232}Th$ and $^{40}K$ from the intensities of the gamma lines emitted.

The results obtained show that the concentrations of radionuclides in the soils of the town of Outjo vary from 11. 7 ± 1.6 to 29. 8 ± 2.0 Bq $kg^{-1}$ with an average of 20.5 ± 3.5 Bq $kg^{-1}$ for $^{238}U$, 15.2 ± 1.8 to 58.3 ± 4.2 Bq $kg^{-1}$ with an average of 31.4 ± 8.9 Bq $kg^{-1}$ for $^{232}Th$ and 206.2 ± 12.9 to 819.6 ± 31.9 Bq $kg^{-1}$ with an average of 350.6 ± 124.6 Bq $kg^{-1}$ for $^{40}K$. The average concentrations for $^{238}U$ and $^{40}K$ are lower than the worldwide averages of 35.0 Bq $kg^{-1}$ and 400.0 Bq $kg^{-1}$ respectively. In contrast, the average concentration for $^{232}Th$ is slightly higher than the worldwide average of 30.0 Bq $kg^{-1}$.

The average outdoor air absorbed dose rate due to terrestrial gamma rays at 1m above the ground was found to be 43.0 ± 10.6 $nGyh^{-1}$ which is below the worldwide average value of 58.0 $nGyh^{-1}$. Also, the corresponding average effective dose was found to be 0.05 ± 0.01 $mSvy^{-1}$ which is below the maximum permissible limit of 1.0 $mSvy^{-1}$.

These results imply that the background radiation in the town is not high. The average values of $Ra_{eq}$ and $H_{ex}$ are 92.4 ± 22.5 Bq $kg^{-1}$ and 0.25 ± 0.06 which are below the recommended maximum limit of 370.0 Bq $kg^{-1}$ and 1 respectively. Furthermore, the average values obtained for the other hazard parameters are all below the recommended maximum values, thus confirming that the town have normal background radiation so that radiation hazard is negligible in the town. All the results obtained in this study will contribute to the national baseline data of activity concentrations of radionuclides in the soils of Namibia.

# ACKNOWLEDGEMENTS

This thesis would not have been possible without the support of many people. Foremost, I would like to express my sincere gratitude to my supervisors, Prof James Akindele Oyedele and Dr. Gotfried Uiseb for their continuous support and immense knowledge. Their guidance helped me in all the time of research and writing of this thesis. I could not have imagined having better advisors and mentors for my study. I would like to thank Mr Erastus Eight Taapopi, Mrs Monica Mwadinomo Nambinga, Ms Mercy Mbuende and Mr Simon Andrew Shimboyo for their help in this project.

I must also express my very profound gratitude to my family and friends for providing me with unfailing support and continuous encouragement throughout my years of study. I would like to thank Mr Ian Marshman for his contribution to my study also. This accomplishment would not have been possible without them.

All praises are for the ALMIGHTY GOD, whose blessings and graciousness flourished my ideas and endowed me with the strength required to complete this work.

## DEDICATION

This thesis is dedicated to my parents, my sister Olivia and my brother Touno.

# DECLARATION

I, Lusina Venomufenu Hanga, hereby declare that this study is a true reflection of my own research, and that this work, or part thereof has not been submitted for a degree in any other institution of higher education.



| L.V. Hanga | ..... | 22nd November 2019 |
|---|---|---|
| Name of Student | Signature | Date |

## ACRONYMS

RPRG – Radiation Physics Research Group

UNAM – University of Namibia

NRPA – National Radiation Protection Authority

IAEA – International Atomic Energy Agency

ICRP – International Commission on Radiological Protection

HPGe – High Purity Germanium

LET – Linear Energy Transfer

UNSCEAR – United Nations Scientific Committee on the Effects of Atomic Radiation

## LIST OF TABLES

## LIST OF FIGURES

# TABLE OF CONTENTS

# CHAPTER 1

## 1 INTRODUTION

This chapter gives an overview of exposure of natural ionizing radiation, and briefly discusses the statement of the problem, objectives of the study, as well as the significance of the study.

### 1.1 Orientation of the study

Unstable atoms such as Potassium ($^{40}$K), Uranium ($^{238}$U) and Thorium ($^{232}$Th) exist in the soil and they continuously emit ionising radiation. Different types of radiation are emitted by these radionuclides [1, 2, 3]. The radionuclides are the radioactive elements of the natural decay series such as the Uranium series, the Thorium series, Neptunium series, Actinium series and radioactive Potassium [4, 5, 6, 7]. Radionuclides can either be anthropogenic or man-made. A significant component of background radiation to which the population is exposed is due to natural radionuclides and their progeny [1, 2, 3, 4].

When the concentrations of radionuclides in the soil are very high, the background radiation will also be high and could lead to potential health hazards [8]. Radionuclides in soil can be a source of external radiation exposure through gamma-ray emission, whereas internal exposure occurs through the inhalation of radon gas, contaminated particles or ingestion of contaminated food [9].

Namibia is the fifth largest producer of Uranium in the world and therefore there could be elevated background radiation in some important towns in the country [10]. Consequently, the background radiation levels in some towns in Namibia have been studied [2, 4, 6] while those in some other towns such as Outjo have not been studied. Currently, the Radiation Physics Research Group (RPRG) of the Department of

Physics at the University of Namibia (UNAM) is compiling a baseline data of radionuclide concentrations in the soils of Namibia and is therefore interested in the radioactivity in Outjo. It is therefore important to determine the concentrations of the radionuclides $^{238}U$, $^{232}Th$ and $^{40}K$ in the soils of Outjo and find the radiation level in the town as well as the potential radiation hazards.

## 1.2 Statement of the problem

In the protection of the general public from unnecessary exposure to ionizing radiation, adequate data on environmental radioactivity is important for regulatory and advisory purposes. Many studies on the concentrations of radionuclides in the soil have been conducted by RPRG in Windhoek [6] and other towns around Namibia such as Oshakati and the coastal towns of Walvis Bay and Swakopmund [3, 4, 11]. These studies were supported by the National Radiation Protection Authority (NRPA) and the International Atomic Energy Agency (IAEA). However, the town of Outjo has not yet been studied and it is of interest to RPRG. It is therefore necessary to assess radionuclide concentrations in the soils of Outjo and determine the level of background radiation in the town.

## 1.3 Objectives of the study

### 1.3.1 Primary Objectives

The aim of the study was to determine the concentrations of the naturally occurring radionuclides ($^{238}U$, $^{232}Th$ and $^{40}K$) in the soil of Outjo and further determine the associated radiation hazards.

### 1.3.2 Specific Objectives

The specific objectives are to:

a) Determine the concentrations and distributions of the radionuclides $^{238}U$, $^{232}Th$ and $^{40}K$ in the soil of the town of Outjo using gamma spectrometry ;

b) Evaluate different radiological parameters such as the absorbed dose rate in air, the annual effective dose, radium equivalent activity, external, internal and gamma hazards indices ;

c) Determine the background radiation level in Outjo and ascertain whether or not it is within the acceptable levels recommended by the International Commission on Radiological Protection (ICRP);

d) Determine the correlation between radionuclides and provide scientific data that will contribute to a national baseline data library of activity concentrations of radionuclides in the soils of Namibia.

## 1.4 Significance of the study

Outjo is located in the Kunene region and it is 317.2 km from the capital city, Windhoek. This town is popular for livestock farming activities and the inhabitants include the Indigenous people, Western descendants and Europeans. It is the gateway to the western side of the Etosha National Park, and it serves as a stopover for people on their way to the park. This study will provide information on the background radiation of this town which in turn will determine the amount of radiation exposure to the inhabitants of the town. Results from this study will contribute to baseline data which can be used for estimating the change in environmental radioactivity or which might be of interest to policy makers, planners and regulators.

# CHAPTER 2

# 2 LITERATURE REVIEW

In this chapter the literature that forms the basis of this research will be reviewed. The interaction of gamma radiation with matter and the biological effects of radiation are discussed. Also, the detector system and some review of national and international studies on radioactivity in soils are also presented.

## 2.1 The discovery of radioactivity

Nuclear Physics has its beginning in 1896, following the discovery of X-rays in 1890 by Roentgen. Henry Becquerel (1852 - 1908) had the idea that minerals made phosphorescent by visible light might emit X-rays [12]. In his experiment, he wrapped a photographic plate with a mineral containing uranium in a black paper (to exclude light). However, when the plate was developed, it showed images of the crystals of uranium compounds. This implied that the mineral emitted (without any external stimulus) some new kind of radiation [13]. This phenomena was further investigated in 1897 by Marie Currie and her husband Pierre, after they spent some time working on the pitchblende - the ore from which uranium is extracted - and found that it emitted "Becquerel rays" with a much stronger intensity than its uranium content would. The only conclusion was that it contained unknown radioactive components. With the help of her husband, she succeeded in isolating two new radioactive elements. They named the first one Polonium (Po) after Marie's native country of Poland and the second one Radium (Ra) [14, 15].

Further research work by Ernest Rutherford (1871 - 1931) showed that a beam from a radium sample splits into three rays when passed through a strong magnetic or electric field. He established that there existed three different types of radiation, which he

named alpha (α), beta (β) and gamma (γ). This phenomena became known as radioactivity [16]. Radioactivity occurs when unstable nucleus disintegrate or decay with the emission of radiation. The radiation emitted is in the form of particles or electromagnetic waves. New nuclides are formed in the process and particles such as alpha, beta and gamma rays are emitted. Nuclides undergoing spontaneous disintegration are said to be unstable or radioactive [17].

### 2.1.1 Naturally occurring radiation and man-made radiation

Natural background radiation is the amount of radiation that a member of the general population receives from exposure to natural sources [8, 12]. Background radiation has always been part of our environment and therefore a part of life on earth [2]. However, for most individuals exposure to background radiation exceeds ionising radiation from all man-made sources combined [18]. Two main contributors of natural radiation exposures are high-energy cosmic ray particles incident on the earth's atmosphere and radionuclides that originated in the earth's crust and are present around us. Some of the materials are cosmogenic, others are primordial [19, 20].

In addition, people are also exposed to man-made radiation through medical treatments and activities involving use of radioactive material. Radionuclides are also produced as a by-product of the operation of nuclear reactors [12, 18]. Radionuclides are the unstable form of an element that emit radiation to transform into a more stable form [21]. Man-made radionuclides are used in the fields of nuclear medicine, chemistry, manufacturing industry and agriculture [22].

### 2.1.2 Primordial radionuclides

Primordial radionuclides are present in various degrees in the environment and have half-lives comparable to the age of the earth, their decay products (e.g. Lead) exist in

very large quantities [2, 8, 12]. Exposure of the human body to external sources is mainly by gamma radiation from radionuclides and their progeny in the Uranium series, Thorium series and the long-lived radioactive Potassium [23]. Some other primordial radionuclides including those that form part of Uranium-235 series also exist in nature but their contribution to the background radiation exposure is very small. Most elements are stable, however those that are unstable have long half-lives and may decay by emitting alpha, beta and gamma radiation. Half-life is the time it takes for a radioactive nuclide to decay to 50% of its original activity [13]. Each radionuclide have a unique half-life. In this study, Uranium-238, Thorium-232 and Potassium-40 are of major concern. Table 2.1 shows the half-lives of the three primordial radionuclides.

Table 2.1: Half-lives of the primordial radionuclides [24].

| **Radionuclide** | **Half-life (Years)** | **Major radiation emitted** |
|---|---|---|
| $^{238}$**U** | $4.47 \times 10^9$ | alpha, beta, gamma |
| $^{232}$**Th** | $1.405 \times 10^9$ | alpha, beta and gamma |
| $^{40}$**K** | $1.28 \times 10^9$ | beta ,gamma |

The primordial radionuclides with long half-lives undergo transitions, and produce several radioactive products in their respective decay chains. Figure 2.1 shows the Uranium-238 decay chain.

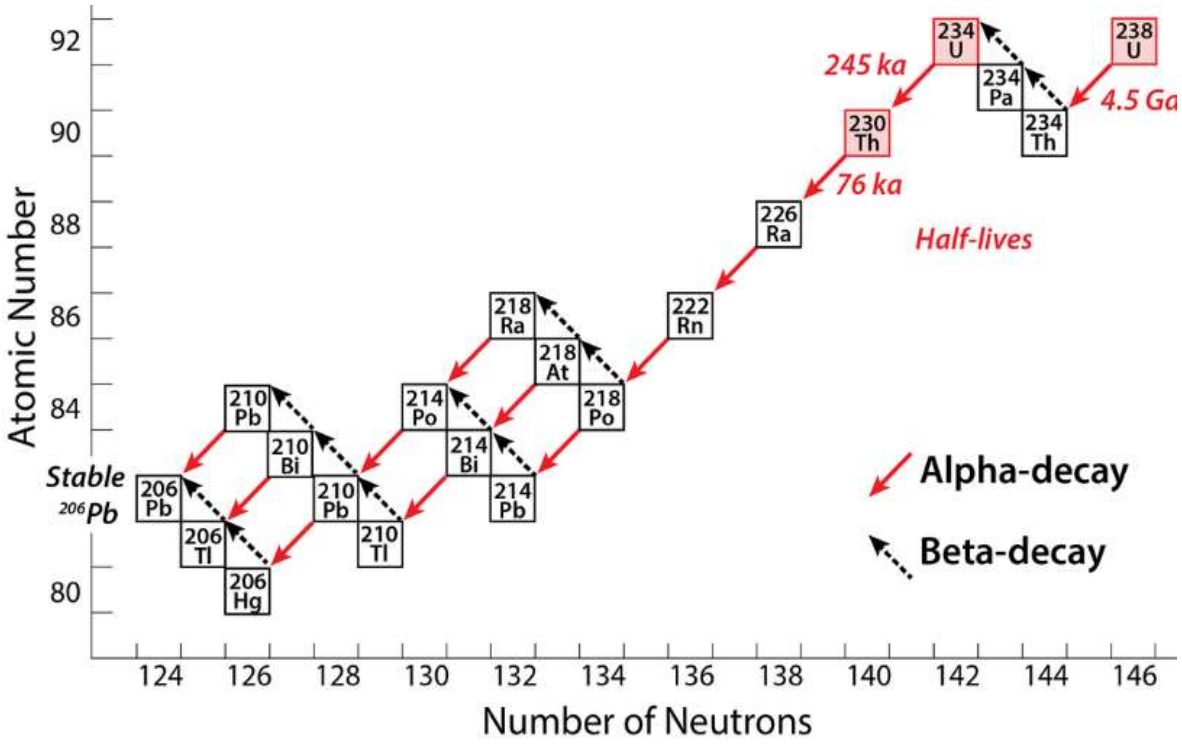


Figure 2.1: Uranium-238 decay series [25].

### 2.1.3 Cosmogenic radiation

Cosmogenic radiation refers to the primary charged and neutral particles produced in extra-terrestrial events such as supernovae and solar flares [26]. The earth is continuously bombarded by high-energy particles that originate in the earth's atmosphere. These cosmic rays interact with the nuclei of atmospheric constituents producing series of interactions and secondary reaction products that contribute to cosmic ray exposure. Cosmic ray interactions produce a number of radioactive nuclei known as cosmogenic radionuclides [23]. Table 2.2 provides information on some common long-lived cosmogenic radionuclides.

Table 2.2: Long-lived cosmogenic radionuclides [19].

| **Nuclide** | **Half-life (years)** | **Decay mode and particle energy (MeV)** | **Atmospheric production rate (atoms $m^{-2}s^{-1}$)** |
|---|---|---|---|
| **$^{3}H$** | 12.32 | $\beta^-$ (0.0186) | 2500 |
| **$^{10}Be$** | $1.52 \times 10^6$ | $\beta^-$ (0.555) | 300 |
| **$^{14}C$** | 5715 | $\beta^-$ (0.1565) | 17000- 25000 |
| **$^{81}Kr$** | $2.2 \times 10^5$ | Ec (0.28) | |
| **$^{36}Ar$** | 265 | $\beta^-$ (0.656) | |

### 2.1.4 Basic constituents of an atom

As it is well known, an atom is the smallest unit of an element. The atom consists of protons, neutrons and electrons as illustrated in Figure 2.2. Both protons and neutrons are referred to as nucleons and they make up the nucleus of the atom. Electrons move around the nucleus in a circular path called orbits [27, 28]. Protons and electrons are positively and negatively charged respectively while neutrons are not charged. The charges on the protons and electrons are exactly the same but of an opposite sign. The mass of the neutron is just about the same as the mass of the proton and they are much larger than that of the electron [29].

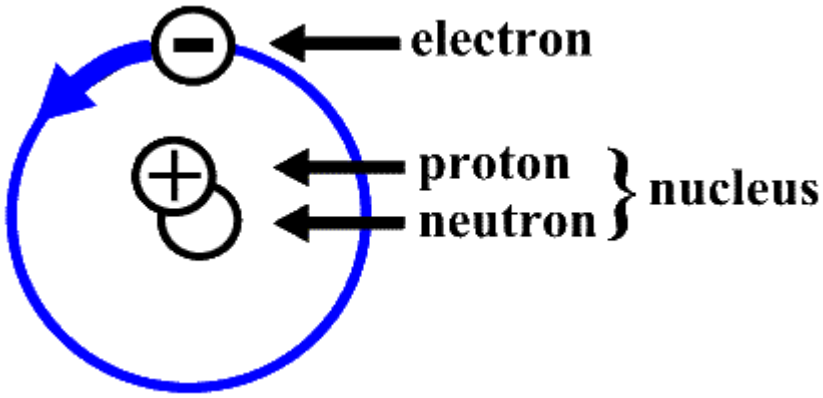


Figure 2.2: Structure of an atom [29].

The following nomenclature apply to the atomic structure.

- The atomic number **Z** is the number of protons in the nucleus and is the same as the number of electrons in a neutral atom.
- The mass number **A** is the number of nucleons in the nucleus and it determines the mass of the atom.
- Atomic mass is the mass of a specific isotope expressed in atomic mass unit (amu), where 1 amu is equivalent to one twelve of the mass of an unbounded neutral atom of Carbon-12 [24].

### 2.1.5 Modes of radioactive decay

An unstable nucleus can give off a particle or ray in order to become a more stable nucleus. Heavy nuclei undergo a combination of alpha (α), beta (β), and gamma (γ) emission. Artificially produced nuclei may also decay by spontaneous fission, neutron emission and even proton and heavy ion emission [30, 31]. Each decay type is discussed below.

(i) Alpha decay (α)

Alpha decay occurs when the nucleus is too large. Heavy nuclei such as $^{208}_{82}$Pb decay by alpha emission. In this decay, two protons and two neutrons are ejected from the nucleus of the radioactive atom as illustrated in Figure 2.3. The two protons and the two neutrons ejected are called alpha particle and it is identical to the nucleus of the helium ($^{4}_{2}$He) atom [32, 33]. The daughter nuclei has an atomic mass four less and an atomic number two less than the parent nuclei. Alpha decay can be written in terms of the parent (X) and daughter (Y) nuclei as

$$^{A}_{Z}X \rightarrow {}^{A-4}_{Z-2}Y + {}^{4}_{2}He \qquad 2.1$$

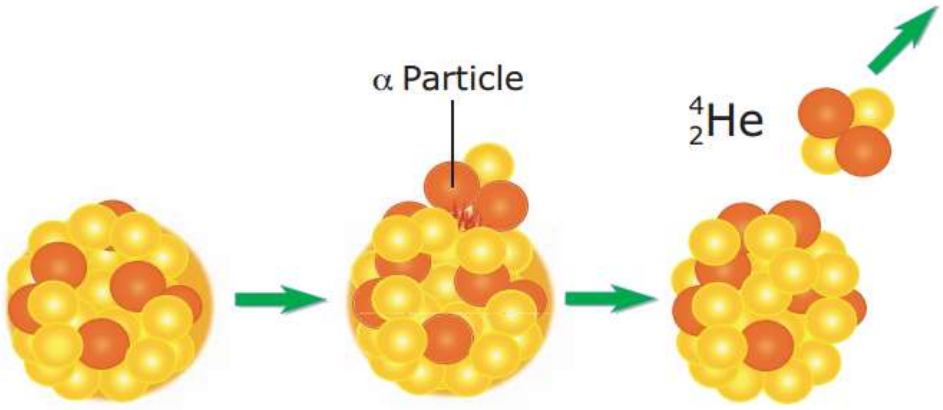


Figure 2.3: Alpha decay [33]

(ii) Beta decay (β)

A nucleus can decay by emitting an electron ($\beta^-$ process) or a positron ($\beta^+$ process). A nucleus can also decay by capturing an electron (electron capture). These processes are known as beta decay [34].

Beta minus ($\beta^-$) decay occurs when the nucleus has too many neutrons relative to protons. In a $\beta^-$ process a neutron in the nucleus changes into a proton, and an electron. An antineutrino is simultaneously created and emitted as shown in Figure 2.4. The

daughter nucleus has an atomic number one more but the mass is the same as the parent nuclei [35]. $\beta^-$ process can be written as;

$$n \rightarrow p + e^- + \bar{\upsilon} \quad 2.2$$

Or

$${}^1_0 n \rightarrow {}^1_1 P + {}^0_{-1} e + \bar{\upsilon} \quad 2.3$$

And in terms of the parent (X) and daughter (Y) nuclei as;

$${}^A_Z X \rightarrow {}^A_{Z+1} Y + e^- + \bar{\upsilon} \quad 2.4$$

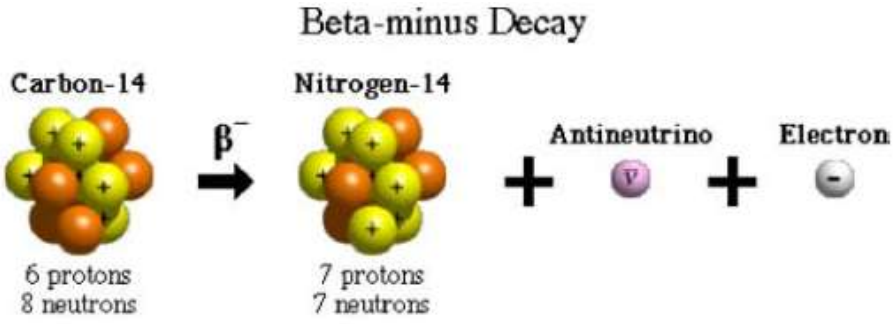


Figure 2.4: Beta minus decay [33]

Beta plus ($\beta^+$) or positron decay occurs when the nucleus has too many protons relative to neutrons. In a $\beta^+$ process, a proton in the nucleus changes into a neutron, and a positron and a neutrino are simultaneously created and emitted as shown in Figure 2.5 [35].The daughter nucleus has an atomic number one less and an atomic mass the same as the parent. $\beta^+$ process can be written as;

$$p \rightarrow n + e + \upsilon \quad 2.5$$

or

$${}^1_1 P \rightarrow {}^1_1 n + {}^0_{+1} e + \upsilon \quad 2.6$$

and in terms of the parent (X) and daughter (Y) nuclei as;

$$ {}^{A}_{Z}X \rightarrow {}^{A}_{Z-1}Y + e + \upsilon \qquad 2.7 $$

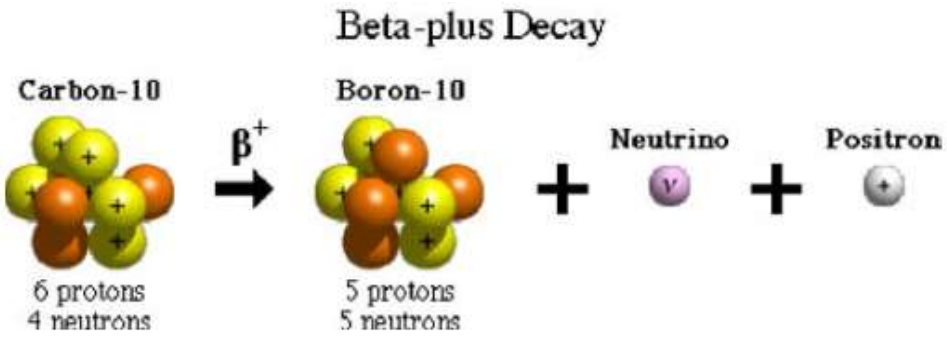


Figure 2.5: Beta plus decay [33]

As in positron emission, electron capture occurs because the nucleus has too many protons relative to neutrons. A proton captures an electron and changes into an electron as illustrated in Figure 2.6 [34]. The daughter nucleus has an atomic number one less and an atomic mass the same as the parent. The process can be written as:

$$ p + e^{-} \rightarrow n + \upsilon \qquad 2.8 $$

and in terms of the parent (X) and daughter (Y) nuclei as;

$$ {}^{A}_{Z}X + e^{-} \rightarrow {}^{A}_{Z-1}Y + \upsilon \qquad 2.9 $$

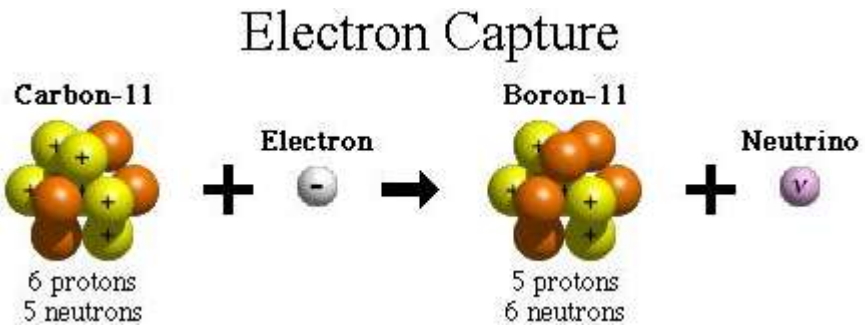


Figure 2.6: Electron capture [33]

(iii) Gamma decay

Gamma rays are electromagnetic radiation and they are not charged unlike α and β particles. When atoms decay by emitting α or β particles to form a new atom, the nuclei of the new atom formed may still have too much energy to be completely stable. This excess energy is emitted as gamma rays as shown in Figure 2.7. Gamma ray photons carry no charge or mass and therefore there is no change in the charge and atomic mass in gamma decay [34, 35]. Gamma decay process (from the excited state to the ground state) can be written as;

$$({}^{A}_{Z}X)* \rightarrow {}^{A}_{Z}X + \gamma \qquad 2.10$$

where * indicates an excited state of the atom.

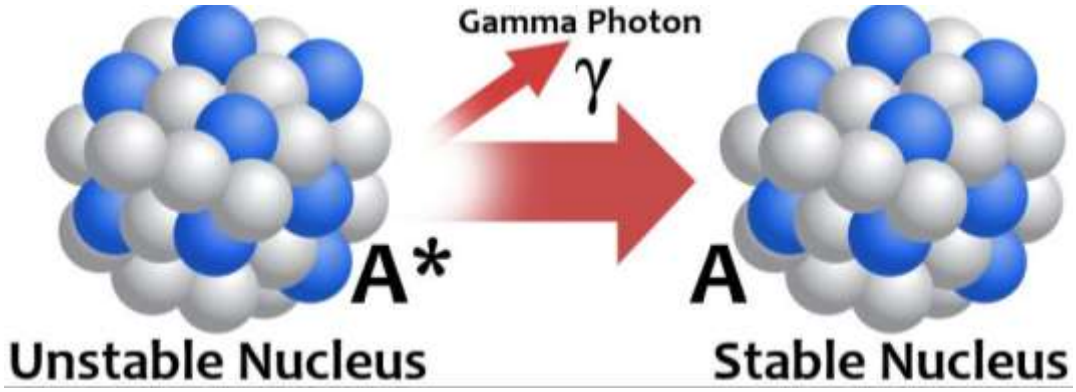


Figure 2.7: Gamma decay [33].

(iv) Spontaneous fission

Heavy nuclei (heavier than ${}^{207}_{82}\mathrm{Pb}$ ) may also decay by spontaneous fission. In this case, the nucleus breaks up into two or more fragments having smaller mass numbers

with the emission of fast moving neutrons. These new fragments are also radioactive and may decay by beta disintegration to become stable [17]. Figure 2.8 illustrate the fission of Uranium-235 after it absorbs a neutron.

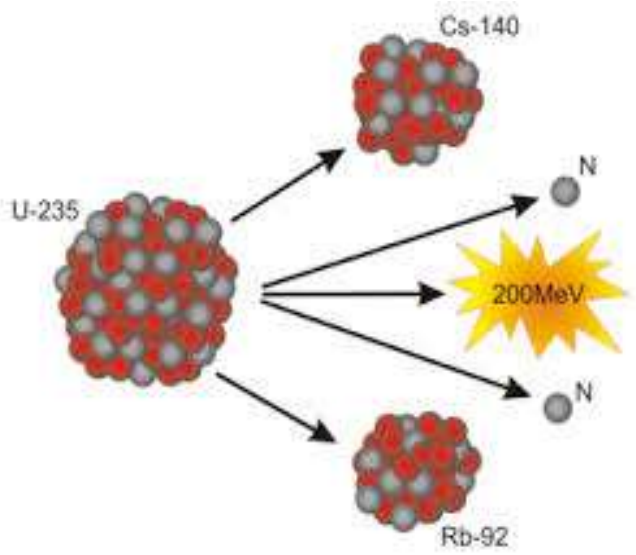


Figure 2.8: Illustration of fission of $^{235}U$.

## 2.2 Interaction of gamma rays with matter

When electromagnetic radiation travels through matter, it can be transmitted without transferring any energy, or its intensity may be reduced by interacting with the traversed medium [36]. The process by which electromagnetic photons (photons are quanta of electromagnetic radiation) are absorbed in matter depends on the incident photon energy and the nature of the target material. In the energy range 0.01 to 10 MeV, gamma rays interact with matter through three processes namely photoelectric effect, Compton scattering and pair production [1, 37, 38]. Details of these processes are discussed below.

### 2.2.1 Photoelectric effect

This is a phenomenon in which a photon interact with an inner bound shell electron in the atom of the medium as shown in figure 2.9. This can take place in the L or K shell

provided that the incident photon energy is more than the binding energy in that shell. The photon transfer its kinetic energy to the electron and this causes the electron to be ejected from the atom [1, 39]. The ejection of an electron creates a vacancy in that shell and leaves an atom in an excited state. This vacancy is filled by an electron from the outer shells whose transition is accompanied by the emission of electromagnetic radiation [39]. In general, the kinetic energy, ($E_k$), of the emitted electron equals the photon energy minus the binding energy of the electron. That is:

$$E_k = h\upsilon - E_B \qquad 2.11$$

where $h\upsilon$ is the energy of the incident photon and $E_B$ is the binding energy of the ejected photo electron.

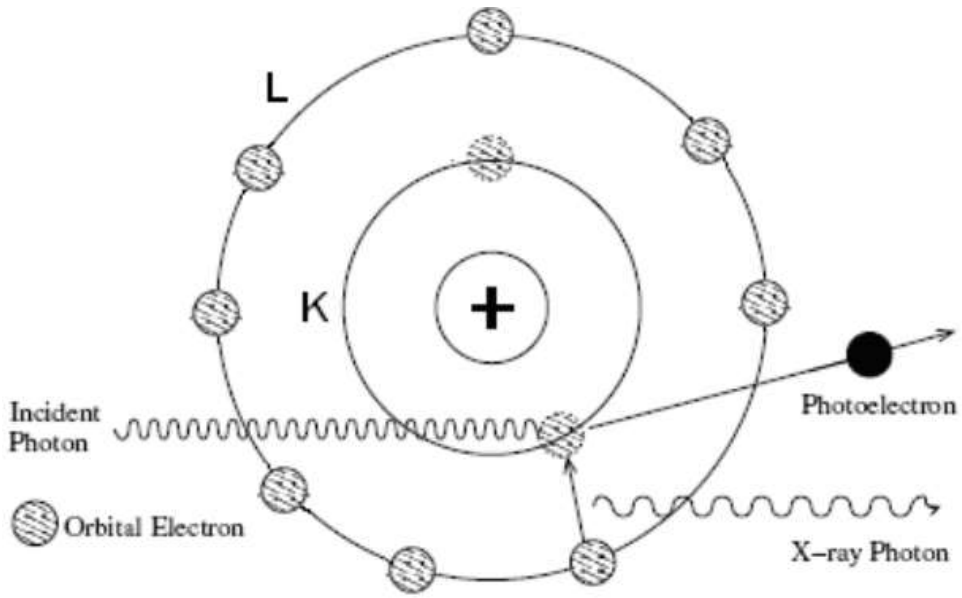


Figure 2.9: Photoelectric effect in an atom [39].

Photoelectric effect is the predominant mode of interaction for gamma rays with relatively low energy and absorbing materials with higher atomic number Z. For this reason, high- Z materials such as lead are used for shielding in gamma ray

spectroscopy [1]. The photoelectric cross-section can be determined by measuring the K-shell X-ray energy and it's given by the following approximation.

$$\sigma_T \cong C \frac{Z^n}{E_\gamma^{3.5}} \qquad 2.12$$

where C is a constant, $E_\gamma$ is the energy of the incident gamma photon, $Z$ is the atomic number of the target atom and $n$ is a number which varies from 4 to 5 depending on the energy of the incident photon.

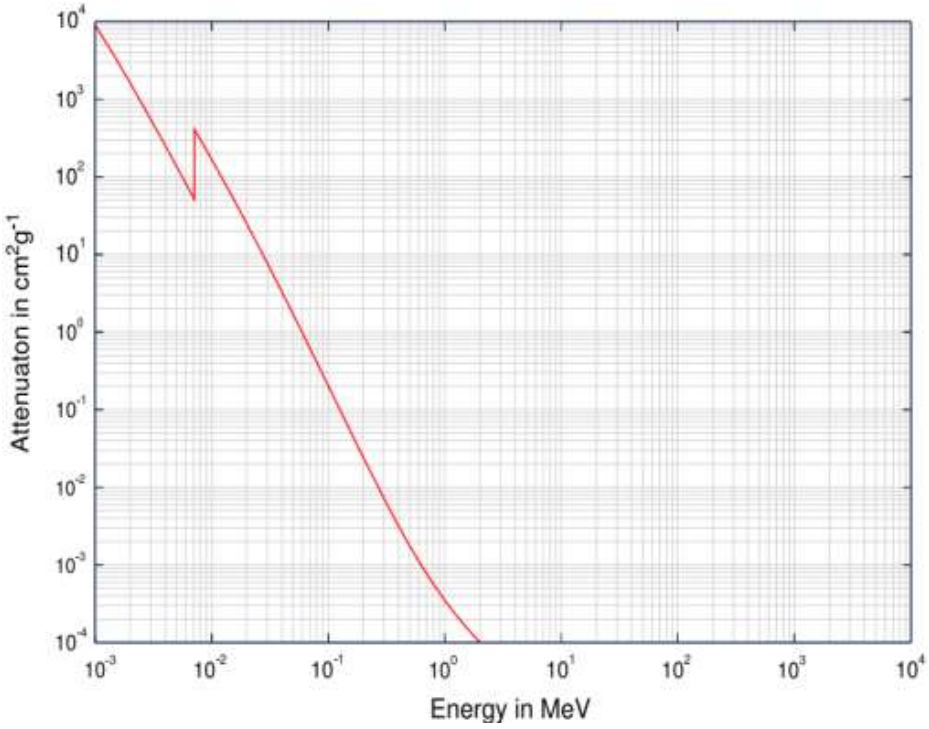


Figure 2.10: Photoelectric effect cross section [24].

### 2.2.2 Compton scattering

In this process, a photon with energy $E_\gamma$ interact with an outer orbital electron in the absorbing material as shown in figure 2.11. In this interaction, the incident photon transfer energy to the atomic electron causing its ejection from the atom. The photon

is than deflected through an angle θ with respect to its original direction. The photon transfer a portion of its energy to the recoil electron. The energy transferred to the electron can vary from zero to a large fraction of the gamma ray energy [1, 2, 37].

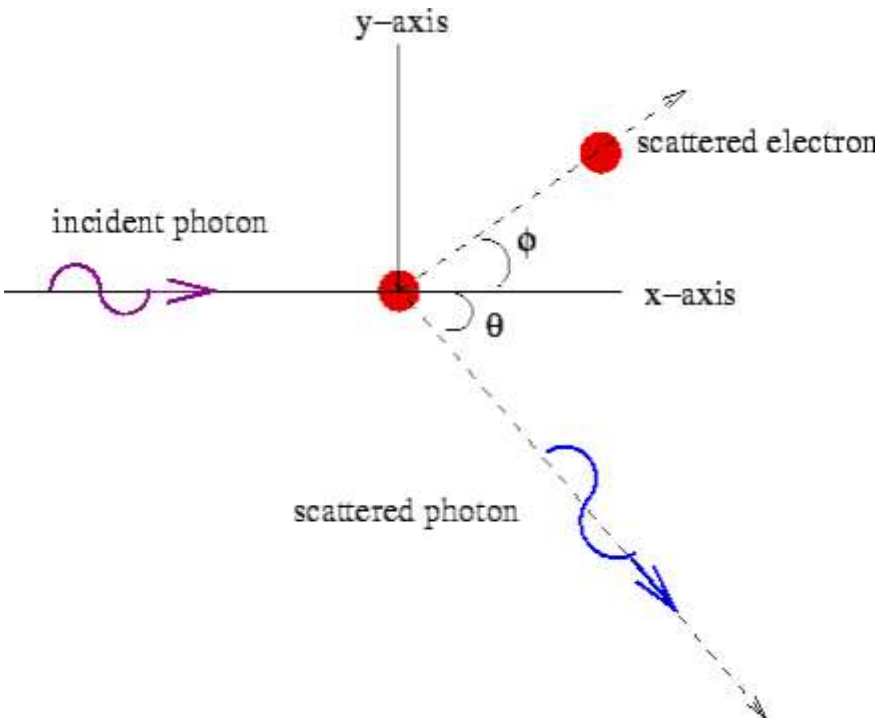


Figure 2.11: Compton scattering [37]

As shown in figure 2.11 the energy of the scattered photon hυ′ is related to the incident photon energy *hυ* by the expression;

$$h\upsilon' = \frac{h\upsilon}{1+\frac{h\upsilon}{m_0c^2}(1-cos\theta)} \qquad 2.13$$

where $m_0c^2$ is the rest mass energy of an electron which is equal to 0.511 MeV. A little energy is transferred by the incident photon and some of the original energy is retained by the photon if the scattering angle θ is very small and even in an extreme case of θ = 180° [1]. Two extreme cases have been identified for Compton scattering and each case is discussed below.

i. If θ = 0° equation 2.13 becomes $h\upsilon = h\upsilon'$ which means that the energy of the scattered photon is the same as the energy of the incident photon.

ii. When θ = 180°, the incident gamma ray is scattered back towards its original direction and the electron recoils in the direction of the incident photon. Also, $h\upsilon'$ is the minimum energy of the scattered photon and the maximum kinetic energy $E_k$ gained by the recoiling electron is given by;

$$E_k = h\upsilon \frac{2\gamma}{1+2\gamma} \quad 2.14$$

The probability of Compton scattering per atom of the absorber depends on the number of electrons available as targets and it increases with the atomic number Z [1]. The angular distribution of the scattered gamma rays can be predicted by the Klein-Nishina formula for the differential scattering cross section $\frac{d\sigma}{d\Omega}$;

$$\frac{d\sigma}{d\Omega} = Zr_0 \left(\frac{1}{1+\alpha\,(1-cos\theta)}\right)^2 \frac{1+cos^2\theta}{2} \left(1 + \frac{\alpha^2(1-cos^2\theta)}{(1+cos^2\theta)[1+\alpha(1-cos\theta)]}\right) \quad 2.15$$

Where $\alpha \equiv \frac{h\upsilon}{m_0c^2}$ and $r_0$ is the classical electron radius $r_0 = \frac{e^2}{4\pi\epsilon_0 mc^2}$.

### 2.2.3 Pair Production

In this process, the entire photon energy is completely absorbed in the material and used up in the creation of an electron-positron pair with the total energy equal to the energy of the photon, and the photon disappears in the process as shown in Figure 2.12 [1, 13, 39, 40]. The energy balance can be written as.

$$E_\gamma = (T_+ + m_+c^2) + (T_- + m_-c^2) \quad 2.16$$

where $T_+$ and $T_-$ are the kinetic energy of the positron and electron respectively, and $m_+$ and $m_-$ are the rest masses of the positron and electron with $m_+ = m_-$. Since $m_+c^2$ and $m_-c^2$ are the rest energy of the positron and the electron and we have,

$$m_+c^2 = m_-c^2 = m_0c^2 = 0.511MeV. \quad 2.17$$

Equations 2.16 and 2.17 show that pair production can only take place if the gamma ray energy exceeds the sum of the rest energies of the positron and electron or $2m_0c^2 = 1.022$ MeV. That is, there is a threshold of 1.022 MeV for the pair-production process. Pair production is important only for photons of high energy and its contribution to the total absorption cross section increases rapidly with energy above 1.022 MeV [40].

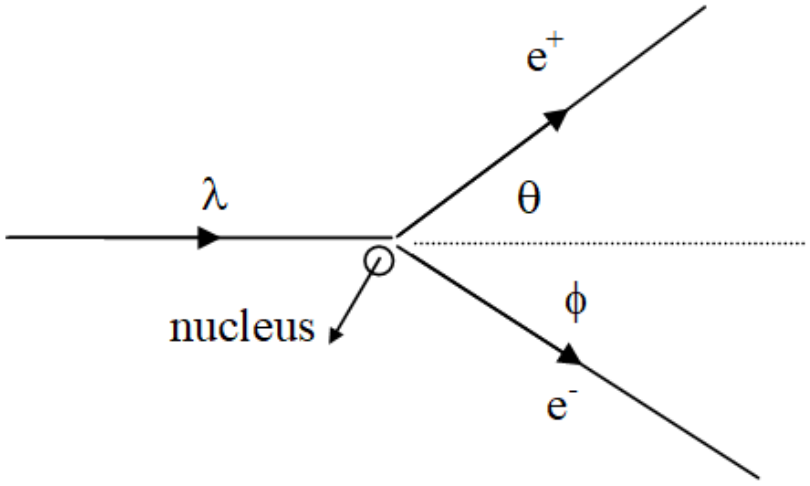


Figure 2.12: Illustration of pair production [25]

The strength of each type of gamma ray interaction depends on the initial gamma ray energy and the atomic number, Z, of the traversed material. The area where each type is most significant is shown in figure 2.13. For low Z materials and gamma energies less than a few hundred keV, the photoelectric effect is the dominant process. Pair production becomes significant at gamma energies above 5 MeV. This leaves the Compton Effect to be most prominent at mid-range energies around 1-2 MeV [1].

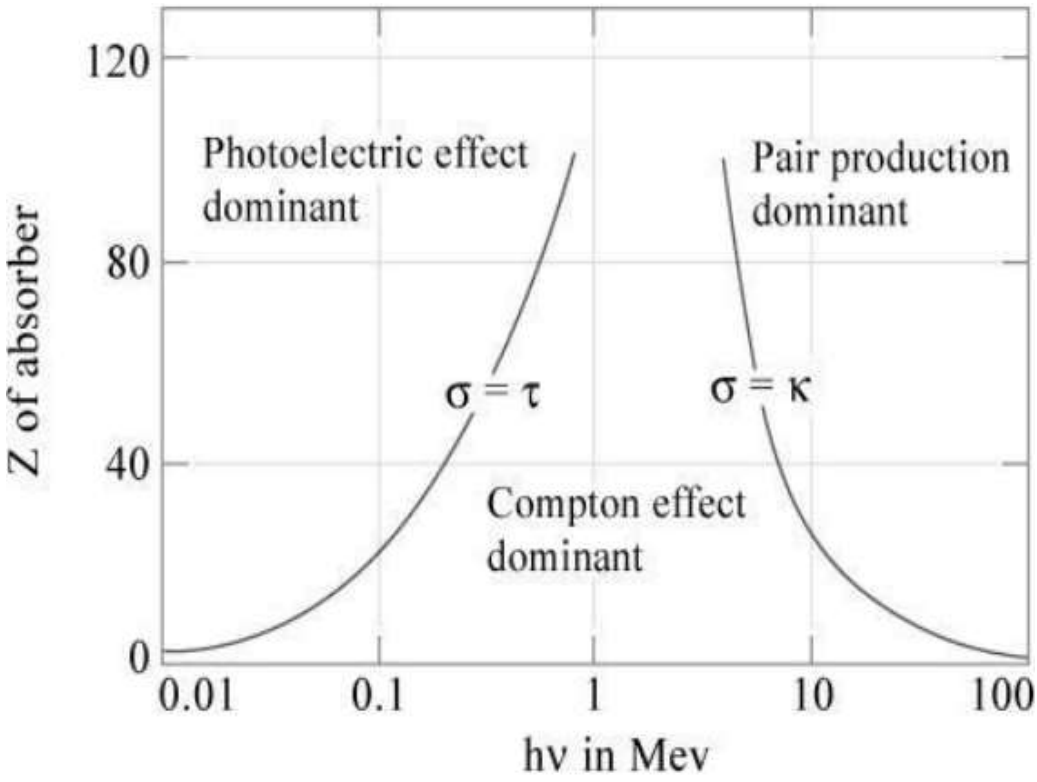


Figure 2.13: The region of dominance of the three gamma-ray interaction processes [2].

## 2.3 Radiation detection and measurements

When radiation enters the detector material, it losses part or all of its energy and release a large number of low-energy electrons from their atomic orbits [1, 17]. The released electrons are collected and formed into a voltage or current pulse for analysis by an electronic circuit. This is the basic principles of operation of most detectors used for nuclear radiation detection and measurement. There is a wide range of detectors and the selection of a radiation detector depends on the measurement requirements such as the radiation type [17]. There are different types of detectors for detecting ionizing radiation and some of these detectors will be discussed below.

### 2.3.1 Gas filled detectors

One of the oldest and most widely used radiation detectors are gas filled detectors. The primary modes of interaction involve ionization and excitation of gas molecules along the particle track. Majority of gas filled detectors are based on sensing the direct ionization created by the passage of radiation [1].

The ionization produced by radiation as it passes through the gas, is utilized in the operation of gas filled detectors. In general, gas filled detectors consist of a closed vessel containing a gas and it's equipped with two electrodes of opposite electrical potentials to which a certain potential is applied as shown in Figure 2.14.

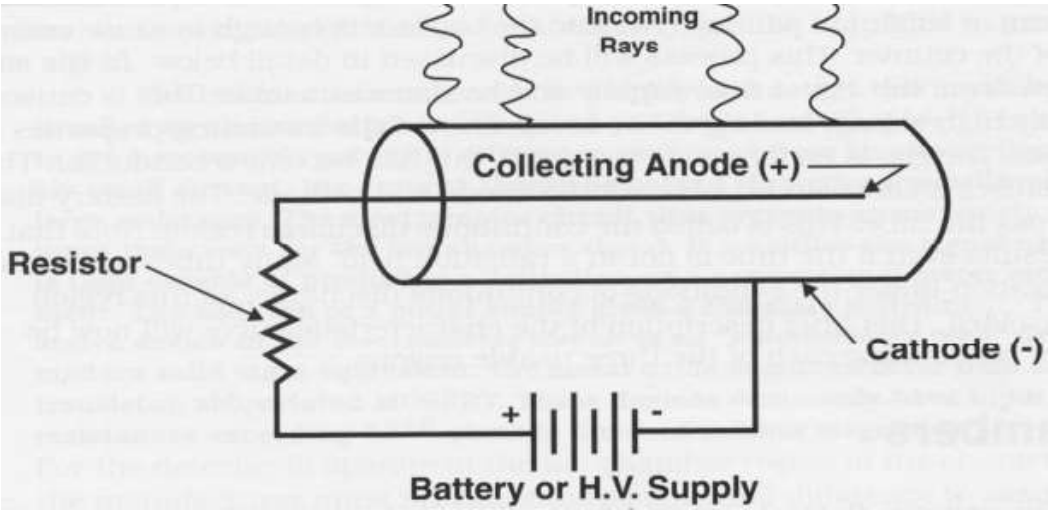


Figure 2.14: Electrical circuit of the gas filled detector [41].

Most of these detectors are usually cylindrical in shape and there is a metal wire at the centre of the detector. The central wire acts as a positive electrode that collects the electrons while the chamber act as the negative electrode [1]. Also, the space between the electrodes is filled with a gas and ionizing radiation passing through the space between the electrodes transfers all or part of its energy by generating electron-ion

pairs that induces current on the electrodes. When electrical charges are collected on the electrode, a measurable electrical current or pulse is produced and then amplified [1, 40, 41]. Gas filled detectors can be operated as Ion chambers, Proportional counters or Geiger Mueller (GM) counters and these detectors take their name from the voltage region in which they operate [41]. The six region characteristic for gas filled radiation detectors are shown in Figure 2.15 and discussed below.

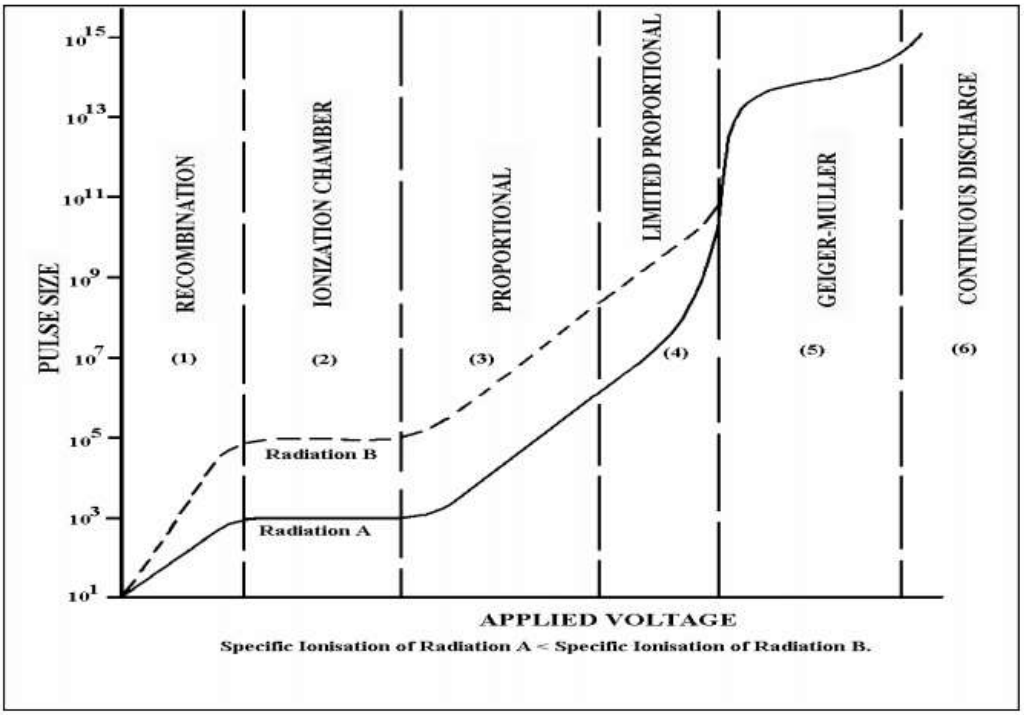


Figure 2.15 : The six regions characteristic curve for gas filled radiation detectors [41].

Region 1 is the Recombination region. This region is not used because the applied voltage is insufficient to collect all of the ion pairs before some of them recombine.

Region 2 is the Ionisation chamber region. As the voltage across the electrode is increased, a voltage range is reached at which all of the ion pairs created in the gas by the ionising radiation are collected before they can recombine. Instruments operating in this region are known as Ionisation chambers.

Region 3 is the Proportional counter region. As the voltage across the electrodes of a gas-filled detector is increased beyond the ion chamber region, the electrons formed by the primary ionisations pick up enough energy during acceleration in the strong electrical field close to the thin central anode wire, to enable them to produce further ion pairs via secondary ionisation. The electrons liberated during secondary ionisation are also accelerated, they gather enough energy to cause further ionisation. The large number of ionisation events formed in the chain reaction is known as an avalanche**,** and creates a single, large electrical output pulse. As the result of gas multiplication, the proportional counter is able to detect individual incident radiations as pulses – hence the name "counter."

Region 4, is known as the Limited proportionality region. This region is not used as the instrument is unstable and calibration is not possible.

Region 5, is the Geiger Muller region. In this region the instrument is operated at high voltages. Inert gases are used as the counting gas. The internal gas pressure is often lower than the atmospheric pressure. Generated electrons are accelerated towards the anode and they produce secondary electrons, a large avalanche of electrons is produced generating a strong electrical signal. A Geiger-counter can detect individual particles and photons.

Region 6, is known as the Continuous discharge Region. In this region the voltage is too high which causes arcing and breakdown of the detector gas.

### 2.3.2 Scintillation detectors

If radiation loses energy in a luminescent material or scintillator, it causes electronic transitions to excited states in the material [40, 42]. The atom in the excited state goes to the ground state directly or via a series by emitting photons, which can be observed

and related quantitatively to the action of the radiation. If the decay of the excited state is rapid, that is in order of $10^{-8}$ or $10^{-9}$, the process is called fluorescence [1].

In order to trap as much light as possible in scintillators, the detector is surrounded by reflecting surfaces. The trapped light is fed into a photomultiplier tube for generation of an electrical signal. A photosensitive cathode convert a fraction of the photons into photoelectrons which are accelerated through an electric field towards another electrode called a dynode. Each electron ejects a number of secondary electrons giving rise to electron multiplication. Secondary electrons are then accelerated through a number of additional dynode stages achieving electron multiplication in the range $10^{7}$ – $10^{10}$ [1]. The magnitude of the final signal is proportional to the scintillator light output, which under the right conditions is proportional to the energy loss that produced the scintillation.

A good scintillator material should efficiently convert the energy deposited by a charged particle or photon into detectable light. Also, it should have a linear energy response and transparent to its own emitted light. Additionally, a good scintillator material should have a photomultiplier tube [42].

### 2.3.3 Semiconductor detectors

Semiconductor detector also known as solid state detector is a reverse biased p-n junction that operates like an ionization chamber [13]. The charge carriers in semiconductor detectors are electron and hole pairs that are created along the path taken by the charged particle through the detector [1]. The large number of generated carriers for a given incident radiation beam produces detectors with a good energy resolution [43]. The usefulness of a semiconductor detector for radiation measurements stems from the special properties obtained when n and p type

semiconductors are brought into good thermodynamic contact creating a diode junction. The characteristic of a semiconductor detector depends on the material used as well as on the way the semiconductor is shaped or treated [43]. The High Purity Germanium (HPGe) detector is a very good example of a semiconductor detector.

### 2.3.4 High Purity Germanium (HPGe) detector

Germanium detectors are semiconductor diodes having a p-i-n structure in which the intrinsic (I) region is sensitive to ionizing radiation mainly X-rays and gamma rays [1, 44]. An electric field extends across the intrinsic region under reverse bias. When gamma photons enter the detector, they interact with the material within depleted volume of the detector. Charge carriers (electrons and holes) are produced and are swept by an electric field to the p and n electrons [45]. The charge which is in proportion to the energy deposited in the detector by the incoming photon is converted into a voltage pulse by a preamplifier [44]. The pulse is further amplified in order to shape it and reduce electronic noise and is sent to the multi-channel analyser (MCA). The MCA sorts the pulses into full energy peaks.

Room temperature operation of germanium detectors of any type is impossible because of the small band gap of 0.7 eV. For this reason, germanium detectors must be cooled to reduce the leakage current to the point that the associated noise does not spoil their excellent energy resolution. Liquid nitrogen ($LN_2$) which has a temperature of 77 $^{\circ}K$ is used for cooling germanium detectors [1].

The detector is mounted in a vacuum chamber which is attached to a $LN_2$ Dewar. The sensitive detector surfaces are thus protected from moisture and condensable contaminants. The energy resolution of germanium detectors is very high but because of their small volume, their sensitivity is low and it may take several minutes to record

a spectrum [1]. Arrangements of p-type and n-type semiconductor detector are shown in figure 2.16.

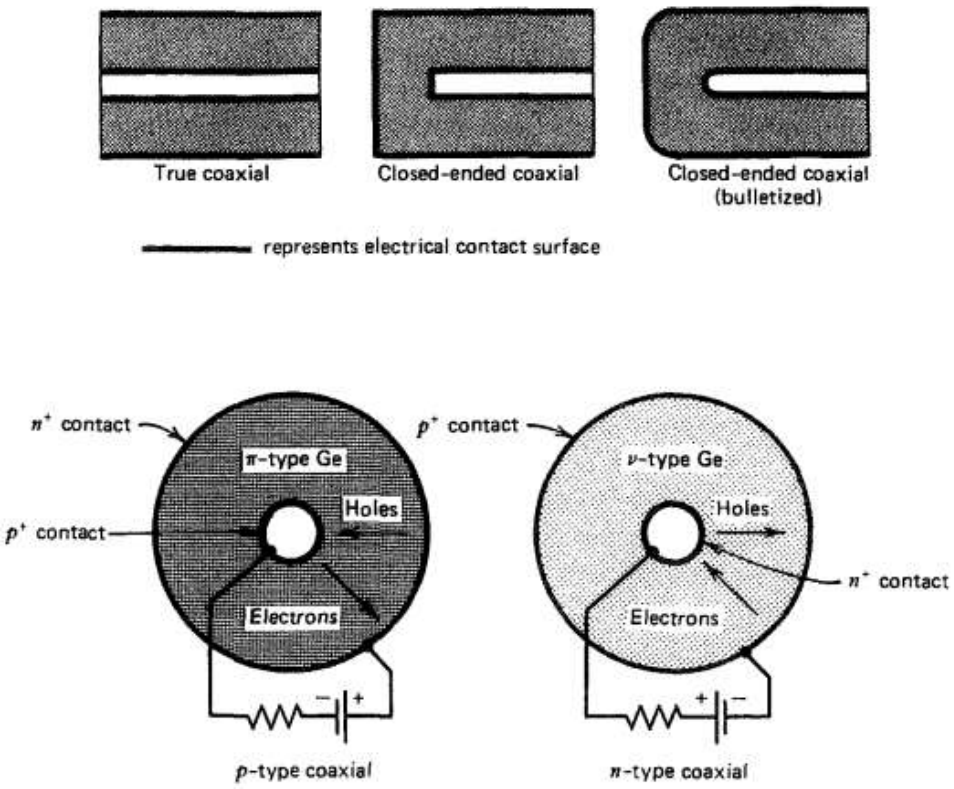


Figure 2.16: Configuration of closed end coaxial n-type and p-type semiconductor detectors and cross sections perpendicular to the cylindrical axis of the high-purity germanium p or n type crystal and corresponding electrode configuration for each type [1].

HPGe detector that are in use exist in two geometries. These geometries are the planar and co-axial HPGe detectors [45]. Planar detectors are used to measure low energy gamma photons in the range 60 – 300 keV and X-rays. Planar detectors are also known as low-energy photon spectrometers. Co-axial detectors have a large active volume that makes them most appropriate for detection of high energy gamma radiation in the

range 300 – 2000 keV [45]. A co-axial germanium detector was used in this study, and figure 2.17 shows a block diagram of gamma spectroscopic system.

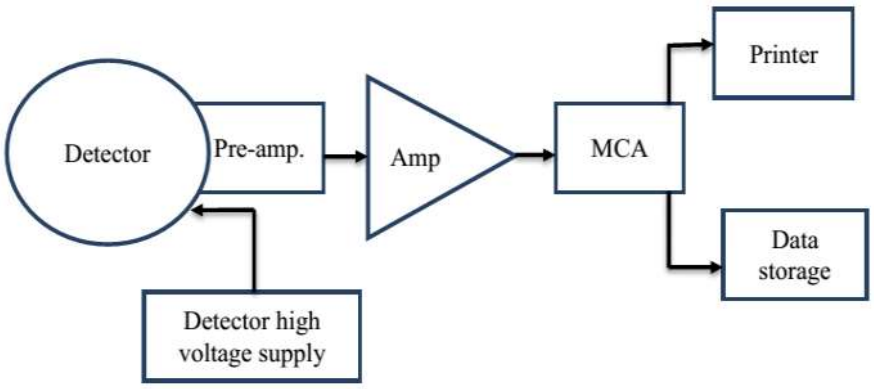


Figure 2.17: Block diagram of gamma spectroscopic system [2].

### 2.3.5 Interaction of Gamma radiation with detector crystal

There are three main processes through which gamma rays interact with matter. These are photoelectric effect, Compton scattering and pair production. In the photoelectric effect, the gamma ray transfer all of its energy to the recoil electron. The recoil electron produces the electron-hole pairs in the detector that yields the output pulse which is proportional to the energy of the gamma ray that interacted with the detector. These events will appear in a spectrum as a full-energy photo-peaks [46]. Photoelectric effect is dominant for incident X-rays or gamma rays with the incident energy of 0 - 150 keV.

Compton cross section is dominant for gamma energy in the range 150 - 8500 keV. Compton effect also contribute to the full energy peak by multiple Compton scattering under the condition that the last interaction is a photoelectric effect and that all the preceding Compton interactions takes place in the germanium crystal. The probability of multiple Compton scattering increases in detectors with a large volume. If the last interaction does not occur by photoelectric effect, or if one of the multiple Compton

interactions takes place outside the sensitive volume of the detector, the pulse will contribute to the Compton continuum [19, 46]. Pair production process also provide a total absorption of the gamma ray energy. The gamma creates an electron-positron pair when it enters the detector. From the law of conservation of mass and energy, the initial gamma energy must be 1.02 MeV since it is the energy required to create both negative and positive electrons.

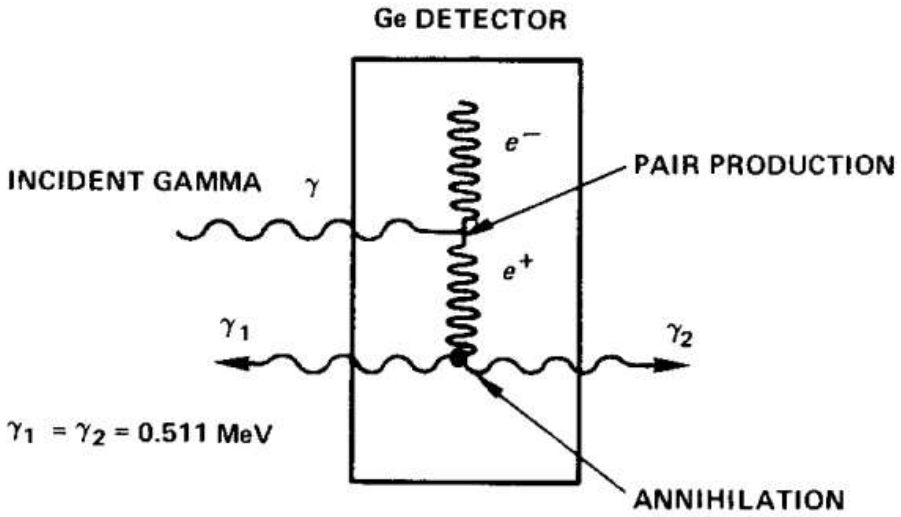


Figure 2.18: Pair production in Ge detector [46].

Figure 2.18 illustrates what happens in the detector during the pair-production process. In the figure the $e^-$ (ordinary electron) will produce a pulse whose magnitude is proportional to the energy of $e^-$ ($E_{e-}$). The positron will also produce a pulse proportional to $E_{e+}$. Since these two these pulses are simultaneously produced, the resulting pulse from the detector would be the total of the two pulses. When the positron enters the detector, the annihilation radiation $\gamma_1$ and $\gamma_2$ are produced. If both $\gamma_1$ and $\gamma_2$ goes beyond the boundaries of the detector without making additional interactions, the energy of exactly 1.02 MeV also escapes from the detector and this is subtracted from the initial total energy that entered the detector. In most cases, only one of the gammas creates a photoelectric interaction in the detector as others escapes.

In such cases, the total energy absorbed by the detector is 0.511 MeV less than the original incident gamma-energy. It is possible that both gammas cause photoelectric interactions without escaping and the incident γ-energy will be absorbed by the detector [46]. Therefore, in the measured spectrum three peaks can be observed for each gamma-energy. These peaks are referred to as full-energy peak, single escape peak, and double-escape peak which can be distinguished by 0.511 MeV increments.

## 2.4 Radiation doses and units

The effect of radiation depends on the duration of exposure, the type of radiation and on the amount of radiation received. The amount is referred to as a dose and measurement of such doses is known as dosimetry. Radiation is measured either as an exposure or as a dose. The dose is the amount of energy absorbed in a system and it is generally regarded as the best way to quantify the irradiation absorption [36]. Different types of doses are discussed below.

(i) Exposure

The radiation exposure is a measure of radiation based on its ability to produce ionization in air under standard temperature and pressure. Exposure is the quantity indicated by many radiation detectors such as the Geiger-Mueller counter. The old unit for exposure is the Roentgen (R), where 1 R is equivalent to 2.58 ×10-4 C/kg air. The international System (S.I) unit for exposure is Coulombs per kilograms (C/kg). The units of exposure is only defined for air and it cannot be used to describe the dose to the tissues [36].

(ii) Absorbed dose

Absorbed dose is the amount of energy absorbed per unit mass of tissue from any kind of radiation. The average absorbed dose ($D_{T,R}$) contributed by ionising radiation of type R and averaged over the volume of a specified organ or tissue T is given by [47];

$$D_{T,R} = \frac{dE}{dm} \qquad 2.18$$

Absorbed dose rate is a physics quantity and its unit the Gray (Gy) is also a physics quantity. Where 1 Gray is equal to I 1 Joule per Kilogram.

(iii) Equivalent dose

For radiation protection and occupational exposure purposes, equivalent dose is used to compare the biological effectiveness of the different types of radiation to tissues. It is the sum of the product of the absorbed dose and the radiation weighting factor $W_R$ for ionising radiation type R [48].

$$H_T = \sum_R W_R D_{T,R} \qquad 2.19$$

Equivalent dose is a protection quantity and its S.I unit is the Sievert (Sv). Radiation weighting factors for different types of radiation are given in Table 2.3.

Table 2.3: Radiation weighting factors $W_R$ [47].

| Radiation Type | Energy Range | $W_R$ |
|---|---|---|
| **Photons (X-rays and gamma rays)** | all energies | 1 |
| **Electrons** | all energies | 1 |
| **Neutrons** | <10 keV | 5 |
| | 10 – 100 keV | 10 |
| | > 100 keV – 2 MeV | 20 |
| | 2 – 20 MeV | 10 |
| | > 20 MeV | 5 |
| **Protons** | > 20 MeV | 5 |
| **Alpha particles, Fission fragments** | | 20 |

(iv) Effective dose

The effective dose is used to estimate the risk of radiation in humans. It is the sum of the product of equivalent dose to each organ or tissue $H_T$ and the tissues weighting factors $W_T$. Tissue weighting factors are used to express the proneness of organs to life threatening radiation related cancer [48].

$$E = \sum_T W_T \sum_R W_R D_{T,R} \qquad 2.20$$

The S.I unit for effective dose is the Sievert (Sv). Also, the effective dose is not a pure physics quantity, and its unit the Sievert is not a physics unit either. The definition for effective dose weighs the physics quantity absorbed dose by weighting factors derived

from radiobiology and radio-epidemiology. Therefore, the effective dose is a protection quantity, a convolution of physics, radiobiology and radio-epidemiology [41].

Table 2.4: Table of tissues and organs weighting factors [41].

| **Organ or Tissue** | **Weighting factors ,$W_T$** |
|---|---|
| **Gonads** | 0.2 |
| **Red Bone marrow** | 0.12 |
| **Colon** | 0.12 |
| **Lungs** | 0.12 |
| **Stomach** | 0.12 |
| **Bladder** | 0.5 |
| **Breast** | 0.5 |
| **Liver** | 0.5 |
| **Oesophagus** | 0.5 |
| **Thyroid** | 0.5 |
| **Skin** | 0.01 |
| **Bone Surface** | 0.01 |
| **Remainder** | 0.05 |
| **Total** | 1.0 |

(v) Collective dose

Collective dose (S) is the total radiation dose incurred by population. The unit for collective dose is the man-Sievert (man-Sv) [36].

$$S = \sum_i E_i N_i \qquad 2.21$$

Where $E_i$ is the average effective dose in the population subgroup i and $N_i$ is the number of individuals in the subgroup i.

Table 2.5: Conversion between units used in radiation protection [25].

| **Physical Quantity** | **S.I unit** | **Non-S.I unit** | **Relationship** |
|---|---|---|---|
| **Activity** | Becquerel (Bq) | Curie (Ci) | 1 Ci = $3.7 \times 10^{10}$ Bq |
| **Exposure** | Coulombs/Kilograms (C/kg) | Roentgen (R) | 1 R = $2.58 \times 10^{-4}$ C/kg |
| **Absorbed Dose** | Gray (Gy) | rad | 1 Gy = 100 rad |
| **Equivalent Dose** | Sievert (Sv) | Rem | 1 Sv = 100 rem |
| **Effective dose** | Sievert (Sv) | Rem | 1 Sv = 100 rem |

## 2.5 Biological effects of ionizing radiation

### 2.5.1 Penetrating powers of radiation

Ionizing radiation can be hazardous to the human body and the effects depends on how the exposure took place. Exposure to the human body can either be through external or internal exposure [49]. Alpha radiation travels only a few centimetres in air and is blocked by a sheet of paper, this makes it unable to penetrate the skin. Alpha particles can be very harmful if an alpha emitting nuclide is taken into the body. Exposure can

be through inhalation of radioactive dust particles from radon gas, it can be swallowed or absorbed through open wounds. Beta particles are more penetrating than alpha particles but are less damaging over equally travelled distances. Beta radiation can penetrate human skin to the germinal layer where new skin cells are produced and if it remains on the skin for a long period of time, they may cause skin injuries. It can be stopped by a sheet of metal such as aluminium or by ordinary clothing. Gamma rays are radiation hazards for the whole body and can easily pass through the human body. Dense materials such as lead and concrete are good barriers against gamma rays [18, 49]. Figure 2.19 illustrates the penetrating powers of different types of radiation.

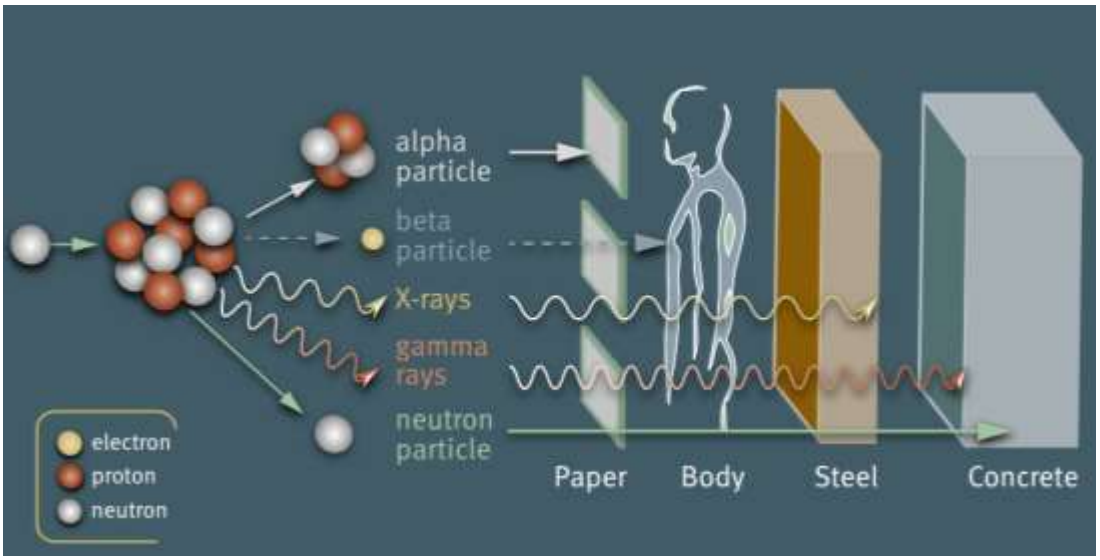


Figure 2.19: Penetrating powers of three types of radiation [18].

### 2.5.2 Linear Energy Transfer (LET)

As discussed earlier, when ionizing radiation travel through matter, they lose energy through different interaction processes along the length of their path. For a particular absorber, the rate of loss of energy depends on the energy, the types of radiation as well as the density of the material [36]. Linear energy transfer (LET) is the density of

energy deposition in a material such as a tissue. It is defined as the average energy deposited per unit length of track of radiation ($\frac{-dE}{dx}$). LET indicates the quality of different types of radiation and it also describe how much energy ionizing radiation transfers to the material traversed per unit length. LET is important because the biological effects of ionizing radiation depends on its average contribution .Charged particles such as alpha particles, protons and heavy ions have high LET because of the high energy they deposit. Uncharged particles such as x-rays and gamma rays have low LET because they deposit low energy. In general, the biological effect of radiation increases with the LET up to a value of about 100 keV/μm [36, 50]. For low LET, the energy travels further but causes less damage to the deoxyribonucleic acid (DNA) helix. For high LET, the energy travels a shorter distance causing more tissue damage such as high single and double strand breakage of the DNA helix [51].

### 2.5.3 Direct and indirect effects

The physical interactions of ionising radiation leads to loss of energy of the radiation and production of ionizations and excitations of atoms and molecules. The atoms and molecules may be converted into free radicals in pico to femto seconds after physical interactions. The radicals react with neighbouring molecules and produce secondary deoxyribonucleic acid (DNA) by reacting with other neighbouring molecules. It is important to mention that, free radicals are fragments of molecules having unpaired electrons which have high reactivity and short life [36]. Electromagnetic and particulate radiations act on cells to cause free radicals and molecular damages through direct and indirect action.

In direct action, the radiation interacts directly with the critical targets in the cell as illustrated by figure 2.20. The atoms of the target cell itself maybe ionized or excited

through coulomb interaction leading to the chain of physical and chemical events that produce the biological damage. Direct action is the dominant process in the interaction of high LET particles with biological materials [52].

In indirect action, the radiation interacts with other molecules and atoms mainly water (since 80% of a cell is made up of water) within the cell to produce free radicals which can through diffusion in the cell damage the critical targets within the cell as illustrated by figure 2.20. When radiation interact with water, reactive free radicals such as water ion ($H_2O^+$) and hydroxyl radical ($OH^\circ$) are produced which can cause damage to the target within the cell [53]. Indirect action is the dominant process in the interaction of low LET particles with biological materials.

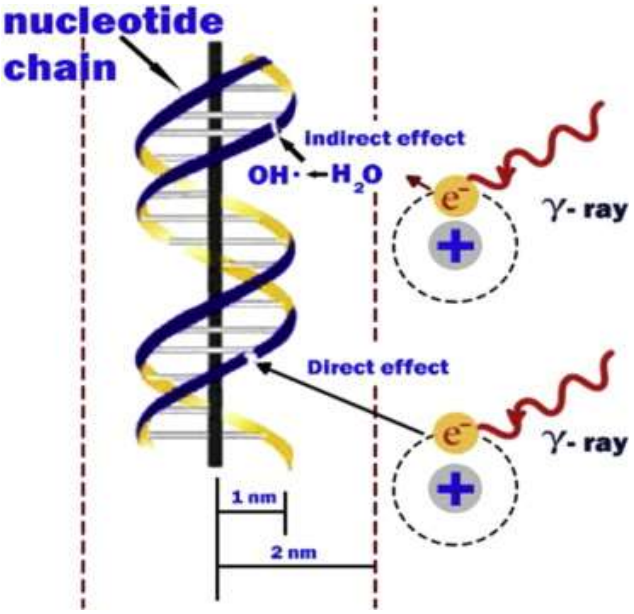


Figure 2.20: Direct and Indirect action of ionizing radiation [52].

### 2.5.4 Health effects of ionising radiation

The biological effects of ionising radiation can be divided into two general categories, stochastic and deterministic effects [54]. Stochastic effects are random and unpredictable effects usually following chronic exposure to low dose radiation over a long period of time. The probability of their occurrence increases with the dose as shown in figure 2.21(a). The induction of cancer and genetic defects are two of the most familiar consequences attributed to stochastic effects [55]. There is also no threshold level of radiation exposure below which we can say with absolute certainty that no cancer or genetic defect will occur and the probability of a cancer or genetic defect occurring doubles when the radiation dose doubles [56]. Deterministic effects are non-random and have a highly predictable response to radiation. They are associated with much higher levels of radiation exposure received over a short period of time. There is a causal relationship between the dose and the effect. There is a threshold dose after which the response is dose-related and they do not occur below the threshold dose as illustrated in figure 2.21(b). Below the threshold dose there is no clinical effect [56, 57].

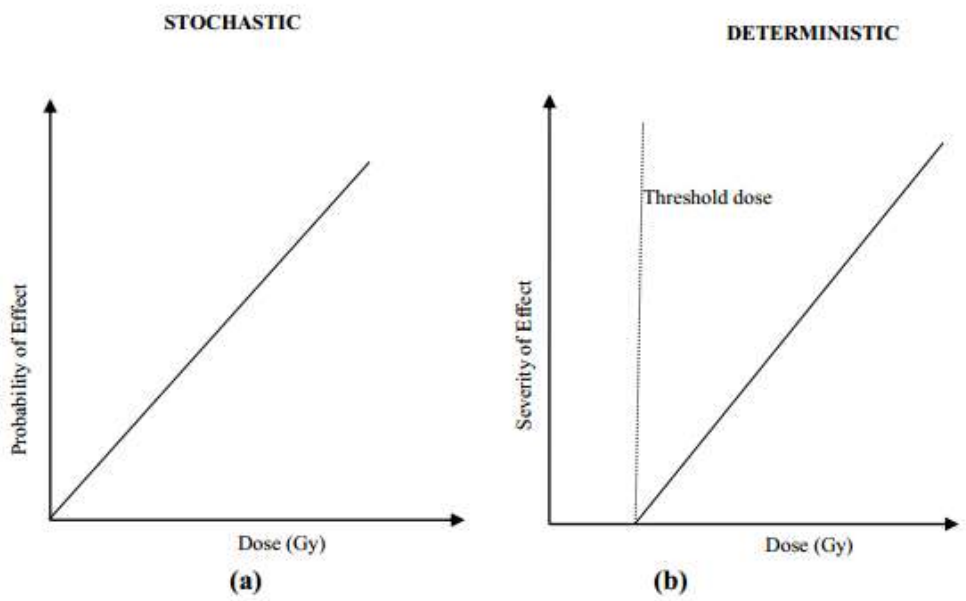


Figure 2.21: Differences between (a) stochastic and (b) deterministic effects of radiation [41]

## 2.6 Radioactivity in soils

The radiation to which the population is exposed comes from many sources. Some of the sources are man-made while some are as a result of human activities. Radiation from natural sources mainly comes from cosmic radiation and from radionuclides present in the soil. The magnitude of these exposures depends on the geographical location. A significant part of the total dose contribution in the form of natural sources comes from terrestrial gamma radionuclides and their corresponding progeny mainly the ones with the half-lives comparable with the age of the earth such as $^{238}U$, $^{232}Th$ and $^{40}K$ [23]. The latter can easily be measured directly using different spectrometers and the results provide an even more extensive evaluation of the background exposure levels in different counties. Measurements of radioactivity are of great interest to many

researchers throughout the world. Table 2.6 summarises the typical contributions of different sources of natural background radiation to the annual dose to the population.

Table 2.6: Average worldwide exposure to natural radiation sources [23].

| **Source of Exposure** | **Annual Effective dose(mSv)** | **Percentage Contribution (%)** |
|---|---|---|
| **Cosmic and cosmogenic** | 0.39 | 16 |
| **External Terrestrial radiation from indoors and outdoors** | 0.48 | 20 |
| **Exposure from Radon and Radon decay products** | 1.26 | 52 |
| **Exposure from Potassium-40 and Uranium and Thorium** | 0.29 | 12 |
| **Total** | 2.42 | 100 |

### 2.6.1 International Studies on radioactivity in soils

Different studies on radioactivity in soil and sediments have been done worldwide. A study on the activity concentrations of natural radionuclides in the Kanyakumari district of southwest India using gamma spectroscopy with NaI (TI) detector found that the mean activity concentrations of $^{232}$Th and $^{40}$K are greater than the world's average values reported by the United Nations Scientific Committee on Effects of Atomic Radiation (UNSCEAR) for areas of normal background radiation [7]. The estimated mean total absorbed dose from the activity concentrations of $^{226}$Ra, $^{232}$Th and $^{40}$K was in the range of 29 ± 14 to 200 ± 30 nGyh$^{-1}$. In a study on natural radioactivity in soils of Baluchistan province of Pakistan using HPGe detector, it was observed that the activity concentrations of $^{226}$Ra, $^{232}$Th and $^{40}$K were in the range of 15-27, 20-37 and 328 - 648 Bq kg$^{-1}$. The calculated absorbed dose rate in air and annual

effective dose were in the range of 35-59 $nGyh^{-1}$ and 0.17 - 0.29 mSv [9]. A systematic survey on natural radioactivity of soils in Slovenia was carried out by using gamma spectrometry. The mean absorbed dose rate was reported to be 260 $nGyh^{-1}$ [5]. In a similar research on the assessment of absorbed dose and radiation hazard index from natural radioactivity in Malaysia, it was found that the average concentrations of $^{238}U$, $^{232}Th$ and $^{40}K$ were below the worldwide average values [58]. Also, the results obtained for the radiation absorbed dose and radiation hazard index were very low, which is a good indication that the place has low background radiation.

### 2.6.2 National studies on radioactivity in soils

Several studies on natural radioactivity levels in the soil have been conducted in Namibia. In a study on natural radioactivity in the soils of Windhoek city using an HPGe detector, results showed that the concentrations of $^{238}U$, $^{232}Th$ and $^{40}K$ varied from 15 ± 1.3 to 37.8 ± 2.1 Bq $kg^{-1}$ for $^{238}U$, 17.5 ± 2.7 to 62.1 ± 3.3 Bq $kg^{-1}$ for $^{232}Th$ and 168.9 ± 15.0 to 784.9 ± 30.1 Bq $kg^{-1}$ for $^{40}K$ [6]. The value of 0.07 ± 0.01 $mSvy^{-1}$ obtained for the effective dose rate was less than the maximum permissible dose of 1 $mSvy^{-1}$ recommended for the public by the International Commission on Radiological Protection (ICRP) [59].

In an assessment of natural radioactivity in the soils of northern Namibia, soil samples were analysed using gamma-ray spectrometry. The mean concentrations for the radionuclides in the towns varied from 7.5 ± 2.3 to 14.2 ± 3.3 Bq $kg^{-1}$ for $^{238}U$, 5.8 ± 2.6 to 24.9 ± 6.2 Bq $kg^{-1}$ for $^{232}Th$ and 52.1 ± 28.7 to 380.1 ± 112.9 Bq $kg^{-1}$ for $^{40}K$.

A low annual effective dose rate, radium equivalent activity and external hazard index were reported in the studies on natural radioactivity in the soils of uranium-rich towns in western Namibia [4]. In the study, samples collected from three major towns and

holiday settlements were analysed using an HPGe detector. The average activity concentrations varied from 18.6 ± 4.6 to 69.6 ± 26.3 Bq $kg^{-1}$ for $^{238}U$, 23.8 ± 8.4 to 91.1 ± 41.0 Bq $kg^{-1}$ for $^{232}Th$ and 460.3 ± 76.2 to 959.5 ± 194.7 Bq $kg^{-1}$ for $^{40}K$. In another study, soil samples collected from Walvis Bay and Swakopmund were also analysed using an HPGe detector. It was reported that the average concentrations of $^{226}Ra$, $^{232}Th$ and $^{40}K$ were 30.4 ± 11.3 Bq $kg^{-1}$, 32.6 ±10.1 Bq $kg^{-1}$ and 203.6 ± 27.0 Bq $kg^{-1}$ respectively in Walvis Bay. Also, the average concentrations of the radionuclides $^{226}Ra$, $^{232}Th$ and $^{40}K$ in Swakopmund were found to be 99.6 ± 24.4 Bq $kg^{-1}$, 90.9 ± 31.1 Bq $kg^{-1}$ and 553.1 ± 107.2 Bq $kg^{-1}$ respectively [3].

Although natural radioactivity has been studied in the soils of some towns in Namibia, there is still a need for studies in other towns in order to determine the concentrations and distributions of the radionuclides $^{238}U$, $^{232}Th$ and $^{40}K$ in the soils of the towns and Namibia. The activity concentrations can be used to calculate the associated radiation hazards in order to determine exposure levels of people to terrestrial gamma radiation from the primordial radionuclides in the ground.

# CHAPTER 3

# 3 MATERIALS AND METHODS

In this chapter, the study area and the materials used as well as sample preparation are discussed. The detector system used in the measurement and the calculations of activity concentrations and radiation hazard indices are also discussed.

## 3.1 Study area

Outjo is located in the Kunene region and it is approximately 317 km from the capital city. It is situated in northern Namibia as shown in Figure 3.1. The name of the town (Outjo) is an Otjiherero name meaning *small hills* which is derived from the surrounding topography [60]. The town was built by Germans in 1897 as a military base in order to explore the northern area of German South West Africa which is now Namibia. Its location coordinates are 20.1128º S and 160.1610° E. The town lies near the Gamkarab cave and it has an estimated population of around six thousand people [61]. Also, the town is nestled among small hills and is best known for being a cattle farming area and the inhabitants include the Indigenous people, Western descendants and Europeans. The town of Outjo also serve as a gateway to the Etosha National Park through the Andersons gate which is approximately 100 km north of the town.


Figure 3.1: Map of Namibia showing the location of Outjo

### 3.2 Sample collection

The town of Outjo was divided into ten geographical areas as shown in Figure 3.2 and five samples were collected at five different sites across each area making a total of 50 samples. All the sites were away from trees, buildings, railway lines, industrial sites and rivers. The samples were collected from undisturbed sites at a depth of about 2-5 cm using a spade, gloves and a dust mask as shown in Figure 3.3 (a) and (b). About 1kg of each sample was transferred into clean polythene bags. The samples were labelled according to the areas and sites and were transported to the Nuclear Physics laboratory in the department of Physics of the University of Namibia in Windhoek for processing.

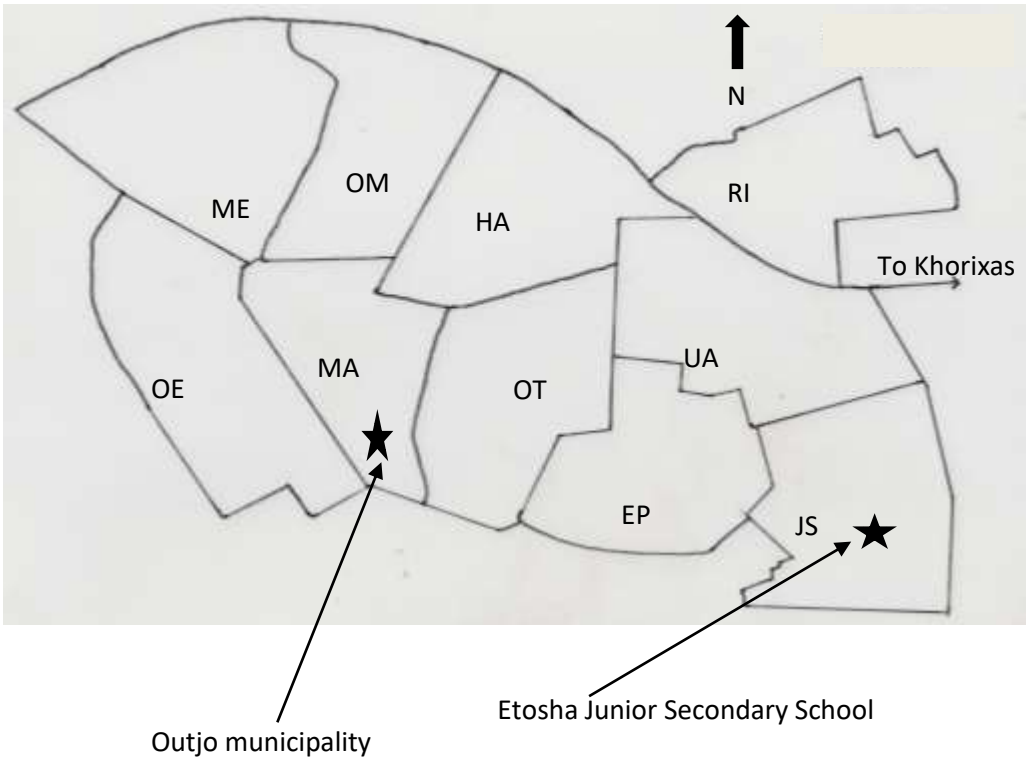


| KEY | |
|---|---|
| **AREA** | **NAME** |
| EP | Etoshaport extension 2 |
| JS | Etosha Junior Secondary School |
| UA | Un-Inhabitant area |
| RI | Industrial area |
| OM | Outjo open market |
| HA | Hospital area |
| OT | Outjo township |
| MA | Municipality area |
| ME | Ministry of education offices |
| OE | Outjo extension 3 |

Figure 3.2: Map of Outjo showing ten geographical areas where soil samples were collected.

(a)

(b)

Figure 3.3: (a) and (b) Sample collection.

### 3.3 Sample preparation

The samples were subsequently left to dry at room temperature for about 72 hours in the laboratory as shown in Figure 3.4. The dried soil samples were pulverised and sieved through a 2 mm mesh screen. The samples were carefully weighed as illustrated in Figure 3.5 (a) and 500 g of each sample was placed in 500 ml polythene bottles and

sealed for about four weeks to ensure radioactive equilibrium between $^{226}Ra$, $^{232}Th$ and their corresponding progeny.

Figure 3.4: Drying of soil samples

**(a)**


**(b)**

Figure 3.5: (a) Determination of the weight of samples and (b) storage of samples

## 3.4 Detector instrumentation and calibration

### 3.4.1 Detector system

The detector used in this study consists of a high-resolution HPGe p-type coaxial detector as shown in Figure 3.6. The detector had a resolution of 1.02 keV Full Width at Half Maximum (FWHM) at 1.22 keV and 1.9 FWHM at 1332 keV, with 25% relative efficiency (Canberra model GC2519). The detector was placed inside a Canberra Model 737 lead shield with a thickness of 10 cm. It also had a graded 1.5 mm copper and 1.0 mm tin lining with an outer jacket of 9.5 mm thick low carbon steel as shown in Figure 3.6. A Model 7915-30 Cryostat (Base Model 7915-30) was used to supply liquid nitrogen ($LN_2$) to the detector, with a Model 2002C Preamplifier as shown in Figure 3.7. Liquid nitrogen was used to cool down the detector and to reduce thermal noise that could be in the system. The system also includes a Model 9660 Digital Signal Processor (housing a Model 2016 Amplifier-TCA, an Analog to Digital Converter (ADC)), an Acquisition Interface Module (AIM

556A) Multichannel Analyser (MCA) as shown in Figure 3.8 (a) and (b). The system also consists of a Model 2100 Bin/Power Supply providing mounting space for a Model 1786 LN2 monitor and a High Voltage Power Supply (HVPS) Model 9645. A block diagram of the HPGe detector system is shown in Figure 2.17. A Genie® 2000 software (version 2.0) was used to analyse the spectra acquired in the measurements [44].

Figure 3.6: HPGe detector in a Lead shield

The High Purity Germanium (HPGe) detector used in this study is a cylindrical germanium crystal with an n-type contact on the outer surface, and a p-type contact on the surface of an axial well. It has a net impurity level of around $10^{10}$ atoms per square centimetre so that with moderate reverse bias, the entire volume between the electrodes

is depleted and an electric field extends across this active region. Photon interaction within the active region produces charge carrier which are swept by the electric field to their collecting electrodes, where a charge sensitive preamplifier converts this charge into a voltage pulse proportional to the energy deposited in the detector [44].

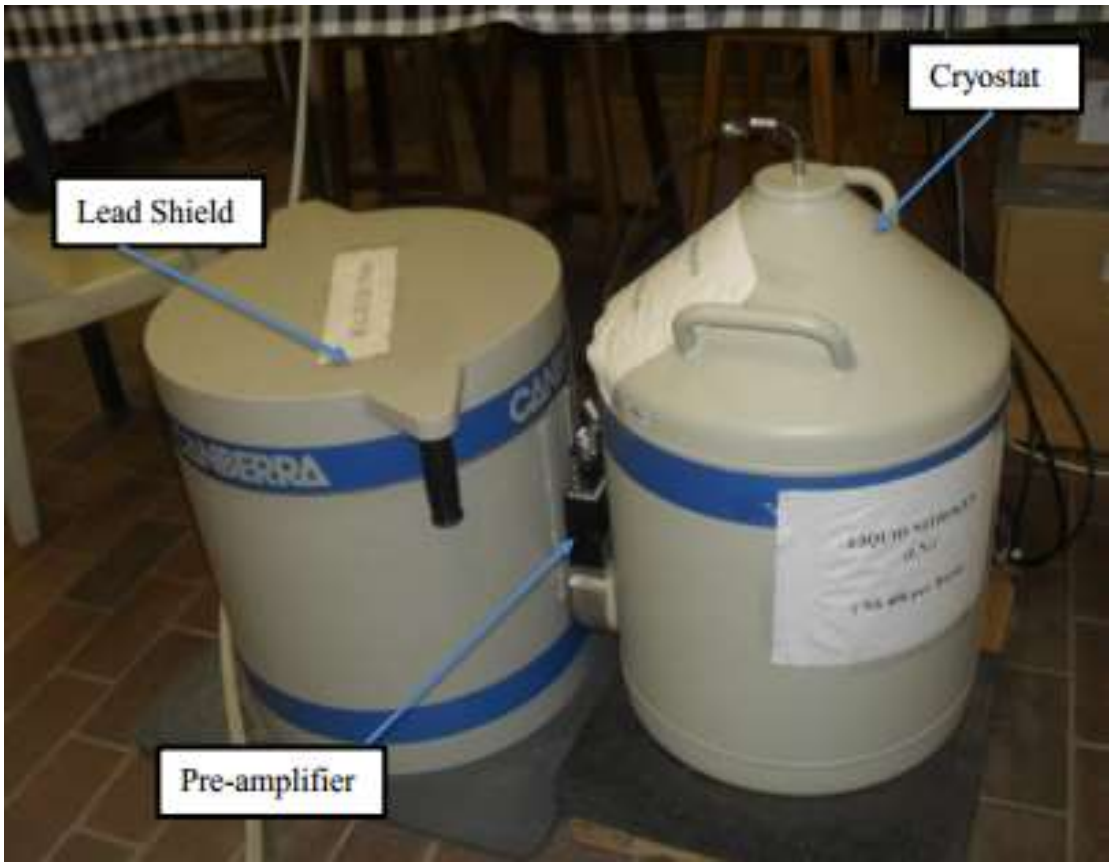


Figure 3.7: Lead shield and Cryostat

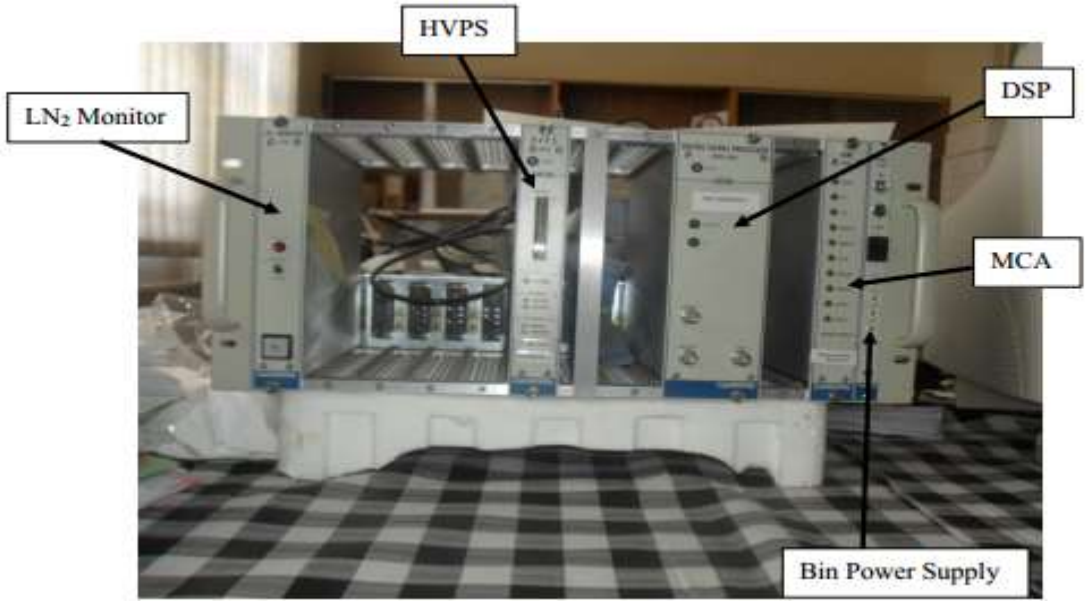


(a)

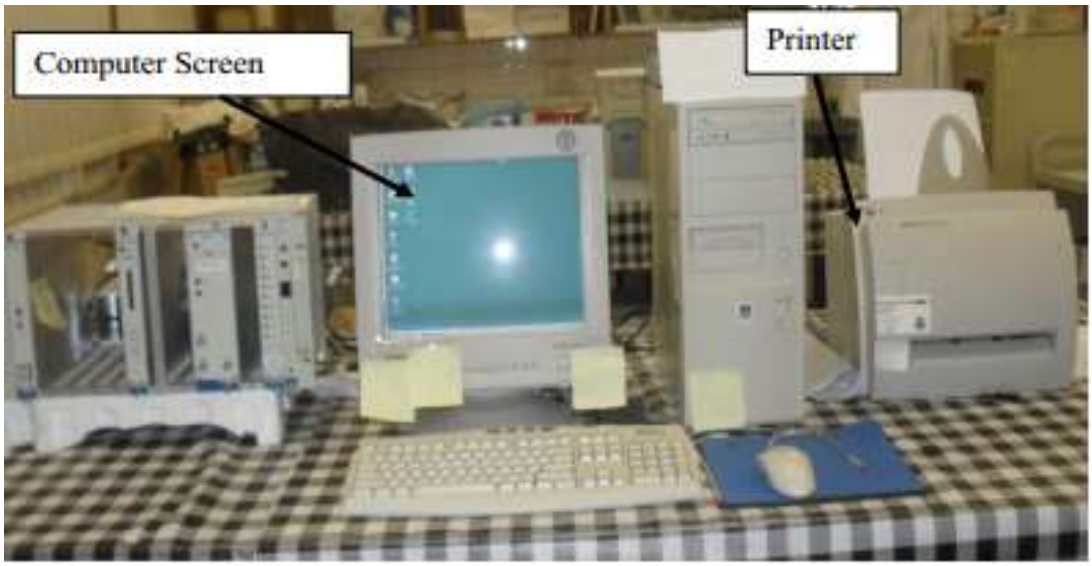


(b)

Figure 3.8: Photographs of the system electronics (a) Liquid nitrogen (LN2) monitor, High voltage power supply (HVPS), Digital Signal Processor (DSP), Multi-Channel Analyser (MCA) and the Power supply to the components. (b) computer screen and printer.

## 3.5 Energy calibration

The energy calibration was done to obtain the relationship between the peak positions in the spectrum and the corresponding gamma-ray energies as shown in Table 3.1. The establishment of this relationship is known as energy calibration and the idea is to identify the energies of radionuclides in a sample. The energy calibration of the detector was done by measuring mixed standard point sources of known radionuclides with well-defined energies within the energy range of interest. The point sources used in the calibration are Sodium-22 ($^{22}$Na), Cobalt-60 ($^{60}$Co) and Ceasium-137 ($^{137}$Cs). The point sources were placed on the detector at once and counted for 1800 seconds. The point sources were selected to cover a wide energy range over which the spectrometer is to be used. The calibration process involved measuring the spectra of the point sources and comparing the measured peak position with energy. This involves matching the peaks in the acquired spectrum with their true energies, then using the Genie 2000 software calibration analysis functions to fit the linear graph as shown in Figure 3.9.

Table 3.1: Point sources used for energy calibration

| **Nuclide** | **Energy (keV)** | **Channel number** |
|---|---|---|
| **$^{137}$Cs** | 661.66 | 1118.13 |
| **$^{60}$Co** | 1173.24 | 1982.55 |
| | 1332.50 | 2251.64 |
| **$^{22}$Na** | 1274.54 | 2153.73 |

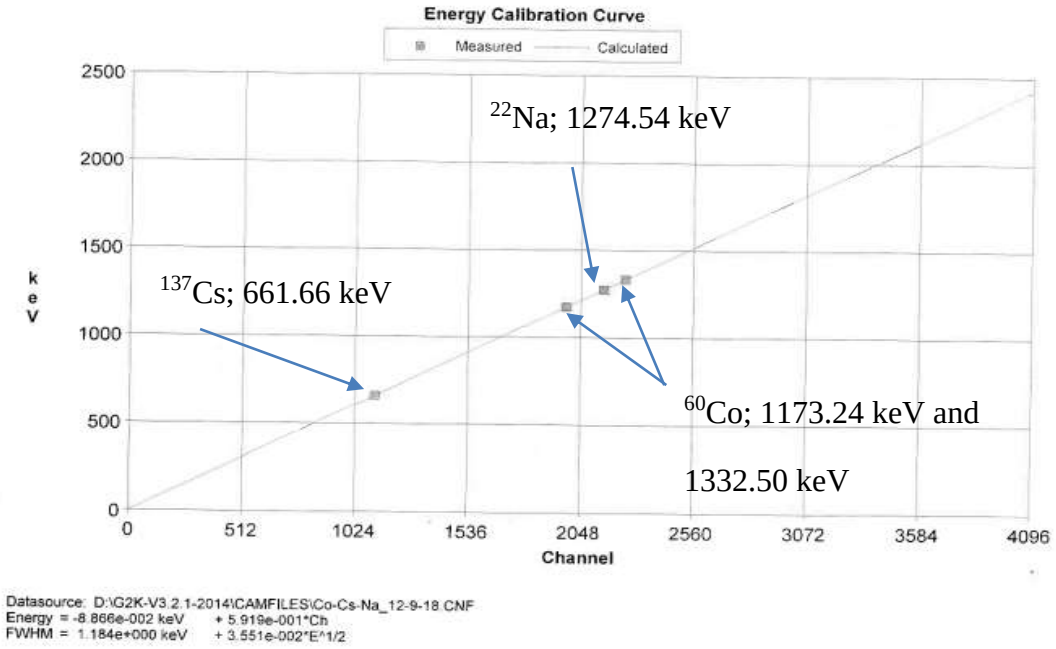


Figure 3.9: Energy calibration curve.

## 3.6 Background counting

It is very important to determine if there is any interference from the detector's surrounding. The background radiation around the detector was counted for 3 hours (10800 seconds) with an empty polythene bottle having the same dimensions as the reference materials and the soil samples. A well-shielded detector was used and the background spectrum was stored in the MCA. Figure 3.10 shows the spectrum obtained from background measurements. The spectrum obtained showed that the background radiation was low, there are no energy peaks corresponding to those of $^{238}$U, $^{232}$Th and $^{40}$K. The background radiation was also counted for 12 hours and the result obtained was similar to that in Figure 3.10.

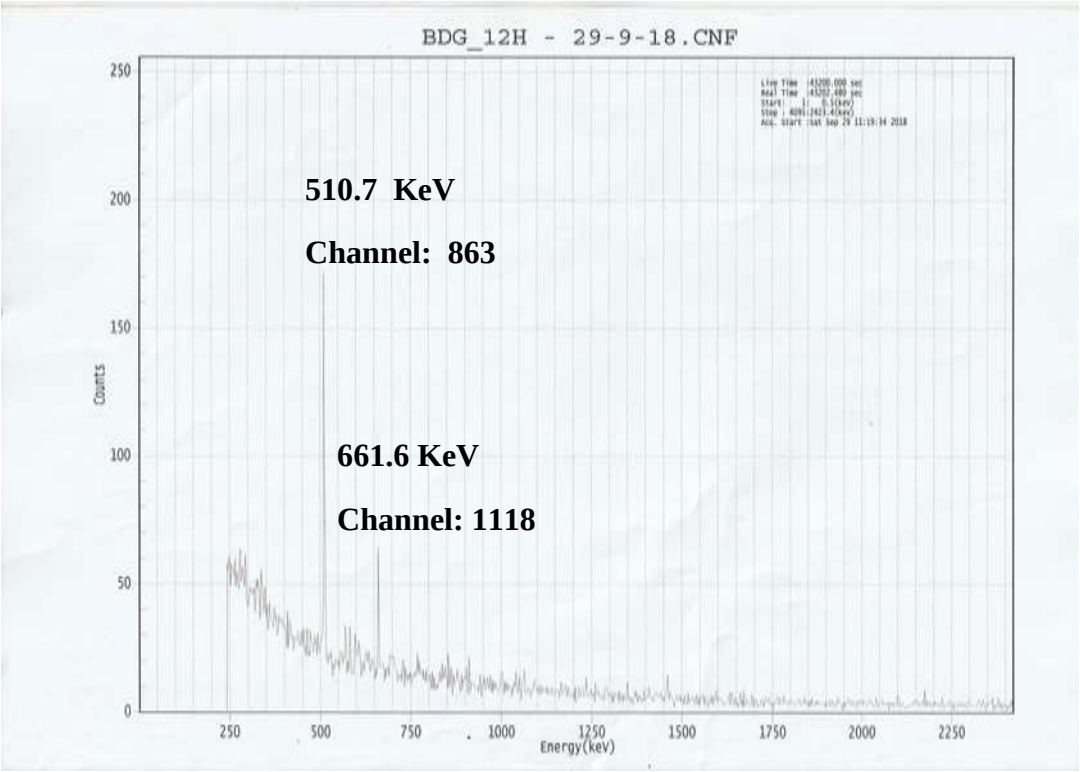


Figure 3.10: Example of background spectrum from HPGe detector system.

### 3.7 Measurement on reference materials

The International Atomic Energy Agency (IAEA) reference materials RGU-1, RGTh-1 and RGK-1were analysed using the HPGe detector. The reference materials standards contained 500g of $^{238}U$, $^{232}Th$ and $^{40}K$ as shown in Figure 3.11. The standards were placed on the detector one at a time and the radiation emitted was counted for 10800 seconds. The spectrum obtained for each reference material was analysed using Genie 2000 Gamma Acquisition software to determine the peak energy and net area of each peak. Radionuclides present in the soil samples could easily be identified by comparing their spectra with those of the reference materials.

Figure 3.11: IAEA certified reference material RGK-1, RGTh-1 and RGU-1.

### 3.8 Measurement on soil samples

The radiation emitted by each of the 50 soil samples were measured using an HPGe detector. Each sample was placed directly on the detector and the radiation or spectra emitted was counted for 3 hours (10800s) as shown in Figure 3.12. Also, the date of measurement on each sample, the sample number and counting period were recorded. Five samples were analysed every working day. The same geometry and counting time interval used for taking measurements on the reference materials were used for taking measurements on the samples. All the spectra were stored in the computer.

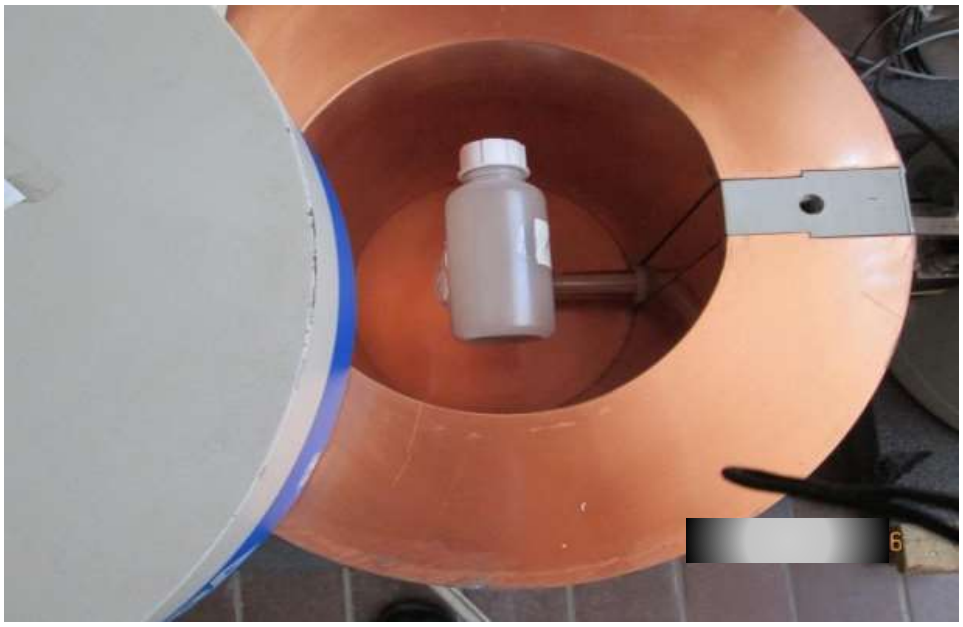

Figure 3.12: Soil sample on the HPGe detector ready for counting.

### 3.9 Determination of activity concentrations

The activity concentrations of the radionuclides $^{238}$U, $^{232}$Th and $^{40}$K in the soil samples were determined using gamma spectrometry. The net peak area under the peak is directly proportional to the specific activity concentration of the radionuclide in the sample [16]. The activity concentrations of $^{238}$U and $^{232}$Th were determined from the intensity of the 609 keV gamma transition line of $^{214}$Bi and the 911 keV gamma line of $^{228}$Ac respectively. Similarly, the concentration of $^{40}$K was determined directly from its characteristic gamma ray energy peak at 1460 keV [62]. Since the net peak area A is proportional to the specific activity concentration C, then this relationship can be written as;

$$A \propto C$$

or

$A = KC$

$\therefore K = \frac{A}{C}$, where K is a constant for a given element.

Therefore for a given element X (e.g. $^{238}U$), in a standard,

$$K^{X}_{standard} = \frac{A^{X}_{standard}}{C^{X}_{standard}} \quad (3.1)$$

Similarly, for element X (e.g. $^{238}U$) in the sample,

$$K^{X}_{sample} = \frac{A^{X}_{sample}}{C^{X}_{sample}} \quad (3.2)$$

or

$$C^{X}_{sample} = \frac{A^{X}_{sample}}{K^{X}_{sample}} \quad (3.3)$$

Since $K^{X}_{standard} = K^{X}_{sample}$ for a given element X, then replacing $K^{X}_{sample}$ with $K^{X}_{standard}$ in equation 3.3 we get that;

$$C^{X}_{sample} = \frac{A^{X}_{sample}}{K^{X}_{standard}} \quad (3.4)$$

$C^{X}_{sample}$ is the concentration of a given element X in a sample. Equation 3.4 shows that the concentration of a given radionuclide X in a sample can be determined from the net peak area of the corresponding peak divided by the constant K for the radionuclide X in the standard. Therefore, to determine the concentration of a radionuclide in a given sample the following equation applies.

$$\text{Concentration of radionuclide} = \frac{\text{Net peak area of radionuclide in a sample}}{K^{radionuclide}_{standard}} \quad (3.5)$$

Equation 3.5 was used to determine the concentrations of the radionuclides $^{238}U$, $^{232}Th$ and $^{40}K$ in all the samples. The results obtained were used to calculate the average concentrations of each radionuclide in a given geographical area.

### 3.10 Determination of Radiation hazards and indices

The main objective of this study is not only to determine the activity concentrations of $^{238}U$, $^{232}Th$ and $^{40}K$ (as the concentration only provide information about the quantity of the radionuclides) but also to estimate the radiation exposure dose and to assess the biological effects on humans. The assessment of biological effects or radiological hazards and indices can be considered in various terms. In this study, six related quantities were calculated from the activity concentrations. These are : the absorbed dose rate in air at 1 metre above the ground ($D$); the annual effective dose equivalent from outdoor terrestrial gamma radiation ($H_E$); the radium equivalent activity ($Ra_{eq}$); the external hazard index ($H_{ex}$), the internal hazard index ($H_{in}$) and the gamma index ($I_\gamma$). These radiological parameters can be calculated from the measured activity concentrations of the three main primordial radionuclides in soil samples, using the relations described below.

A measure of the amount of radiation absorbed per unit mass is known as the absorbed dose rate [36]. The absorbed dose rate was calculated using the activity concentrations of the radionuclides in the soil samples. The external outdoor absorbed dose rates due to terrestrial gamma rays at 1 m above the ground was calculated using equation 3.6 [2, 6, 19].

$$D\ (nGyh^{-1}) = 0.462\ C_u + 0.604\ C_{Th} + 0.0417\ C_K \qquad (3.6)$$

where 0.462, 0.604 and 0.0417 are the absorbed dose rate conversion factors for $^{238}U$, $^{232}Th$ and $^{40}K$ in nGy $h^{-1}$/Bq $kg^{-1}$ and $C_{u,}$ $C_{Th}$ and $C_K$ are the activity concentrations for $^{238}U$, $^{232}Th$ and $^{40}K$ respectively.

In order to estimate the radiological risk to which the public is exposed, the absorbed dose rates were used to calculate the annual effective doses ($H_E$) using a conversion factor of 0.7 $SvGy^{-1}$ and an outdoor occupancy factor of 0.2 which assumes that people on average spend approximately 20% of their time per day outdoors as adopted by UNSCEAR report (2000) [23]. Therefore, the outdoor annual effective dose equivalent was estimated by using the following equation 3.7 [42].

$$H_E = D\left(\frac{nGy}{h}\right) \times 8760\left(\frac{h}{y}\right) \times 0.7\,\frac{Sv}{Gy} \times 0.2$$

$$H_E\left(\frac{mS}{y}\right) = (D \times 0.7 \times 0.2 \times 0.008760) \qquad (3.7)$$

The distribution of radionuclides $^{238}U$, $^{232}Th$ and $^{40}K$ in the soil is not uniform. The non-uniform distribution from these naturally occurring radionuclides is due to disequilibrium between $^{226}Ra$ and its decay products. The radionuclide concentrations of $^{238}U$, $^{232}Th$ and $^{40}K$ in the samples can be evaluated by means of a common radiological index named the radium equivalent activity ($Ra_{eq}$). The $Ra_{eq}$ allows the comparison of the specific activities of materials containing different amounts of $^{238}U$, $^{232}Th$ and $^{40}K$ [63]. The radionuclide concentrations have been defined in terms of Radium equivalent activity ($Ra_{eq}$) in Bq $kg^{-1}$ using equation 3.8 [63]. This assumes that 370 Bq $kg^{-1}$ of $^{226}Ra$, 259 Bq $kg^{-1}$ of $^{232}Th$ and 4810 Bq $kg^{-1}$ of $^{40}K$ produce the same gamma-ray dose rate.

$$Ra_{eq} = C_U + 1.43\,C_{Th} + 0.077\,C_K \qquad (3.8)$$

where $C_U$, $C_{Th}$ and $C_K$ are the concentrations of $^{238}U$, $^{232}Th$ and $^{40}K$ as defined earlier. The maximum value of the $Ra_{eq}$ is required to be less than the limit value of 370 Bq $kg^{-1}$ in order to keep the external dose below 1mSv $y^{-1}$.

Another important hazard used to evaluate the hazard of the natural gamma radiation is defined by the external hazard index ($H_{ex}$). It is used to estimate the indoor radiation dose due to the outward exposure to gamma radiation released by the natural radionuclides in the formation of building materials [64]. In order for the radiation hazard to be insignificant, the value of external hazard index must not exceed the limit of unity. The maximum value of $H_{ex}$ equal to unity corresponds to the upper limit of radium equivalent activity [65]. It was calculated for each sample using the following equation.

$$H_{ex} = \frac{C_U}{370} + \frac{C_{Th}}{259} + \frac{C_K}{4810} \tag{3.9}$$

where $C_U$, $C_{Th}$ and $C_K$ are the activity concentrations for $^{238}U$, $^{232}Th$ and $^{40}K$. Also, secular equilibrium was assumed between $^{238}U$ and $^{226}Ra$.

Inhalation of alpha particles emitted from short-lived radionuclides such as radon ($^{226}Rn$, the daughter products of $^{226}Ra$) and thoron ($^{220}Rn$, the daughter products of $^{224}Ra$) are also hazardous to respiratory tract. This hazard can be quantified by the internal hazard index ($H_{in}$) and it is calculated by the following relation [18];

$$H_{in} = \frac{C_U}{185} + \frac{C_{Th}}{259} + \frac{C_K}{4810} \tag{3.10}$$

The $H_{in}$ should be less than unity to provide safe levels of radon and its short-lived daughters and also for the radiation hazard to be considered negligible.

The gamma index, $I_\gamma$, was also calculated using equation (3.11). This index is used to estimate the gamma radiation hazard associated with natural radionuclides. Values of $\mathbf{I_\gamma} \leq 1$ corresponds to an annual effective dose of less than or equal to 1mSv, while $\mathbf{I_\gamma} \leq 0.5$ corresponds to annual effective dose less or equal to 0.3 mSv [66];

$$I_\gamma = \frac{C_U}{300} + \frac{C_{Th}}{200} + \frac{C_K}{3000} \tag{3.11}$$

All the calculations of activity concentrations and radiation hazards and indices for the town of Outjo were done using the Python software as shown in appendix II.

# CHAPTER 4

## 4 RESULTS AND DISCUSSIONS

The main aim of this study was to determine the activity concentrations of the radionuclides $^{238}U$, $^{232}Th$ and $^{40}K$ in the soil samples collected from Outjo using gamma spectrometry and to further determine the radiation hazards associated with these natural radionuclides. The activity concentrations of $^{238}U$, $^{232}Th$ and $^{40}K$ measured in the soil samples collected from different geographical areas of Outjo are presented in this chapter. Radiological hazards and other statistical analysis of the data are also presented.

### 4.1 Radionuclide concentrations in Outjo

The mean and range of activity concentrations of the radionuclides $^{238}U$, $^{232}Th$ and $^{40}K$ in the soil samples collected from the ten geographical areas of Outjo are presented in Table 4.1 and shown in Figure 4.1. The concentration measured in each of the 50 soil samples are shown in Appendix I and the statistics of the results obtained in the measurements are given in Table 4.2. As could be observed in Table 4.1 and figure 4.1, the concentration of $^{238}U$ varies from a minimum of 11.7 ± 1.6 Bq $kg^{-1}$ in the HA area to a maximum of 29.8 ± 2.0 Bq $kg^{-1}$ in the OE area with an average value of 20.5 ± 3.5 Bq $kg^{-1}$ for the town. Similarly concentrations of $^{232}Th$ varies from a minimum of 15.2 ± 1.8 Bq $kg^{-1}$ in the ME area to a maximum of 58.3 ± 4.2 Bq $kg^{-1}$ in the OE area with a mean of 31.4 ± 8.9 Bq $kg^{-1}$. Concentrations of $^{40}K$, its concentration vary from 206.2 ± 12.9 Bq $kg^{-1}$ in the OM area to 819.6 ± 13.9 Bq $kg^{-1}$ in the OE area with an average of 350.6 ± 124.6 Bq $kg^{-1}$. The results of this study were then compared with the worldwide average activity concentrations of $^{238}U$, $^{232}Th$ and $^{40}K$ in soils. According to the UNSCEAR report 2000 [23], the worldwide average activity concentrations of $^{238}U$, $^{232}Th$ and $^{40}K$ are 35, 30 and 400 Bq $kg^{-1}$ respectively.

The concentrations observed in this study for $^{238}U$ and $^{40}K$ are lower than the worldwide averages of 35 Bq $kg^{-1}$ and 400 Bq $kg^{-1}$ respectively. In contrast, the average concentration for $^{232}Th$ is slightly higher than the worldwide average of 30 Bq $kg^{-1}$. The high concentration of $^{232}Th$ could be attributed to its natural abundance in the soil of the area. In each of the ten areas, $^{40}K$ has the highest average activity concentration while $^{238}U$ has the lowest average activity concentration as could be observed in Figure 4.1.

Table 4.1: The average activity concentrations of $^{238}U$, $^{232}Th$ and $^{40}K$ in different geographical areas of Outjo. The range of values is given in parenthesis.

| **Area** | **Mean radionuclide concentrations [Bq kg$^{-1}$]** | | |
|---|---|---|---|
| | **$^{238}U$** | **$^{232}Th$** | **$^{40}K$** |
| EP | 21.3 ± 4.0 (15.2 – 25.8) | 35.7 ± 9.1 (20.2 - 42.5) | 326.8 ± 33.9 (269.8 – 352.3) |
| JS | 24.3 ± 3.1 (20.7 – 28.4 ) | 30.5 ± 5.4 (22.5 – 35.2) | 314.5 ± 53.4 (243.4 – 385.4) |
| UA | 20.5 ± 0.9 (19.5 – 21.5) | 34.4 ± 3.3 (31.3 – 39.8) | 323.3 ± 41.6 (289.2 – 387.9) |
| RI | 18.1 ± 2.2 (15.9 – 22.0) | 23.8 ± 2.2 (21.4 – 26.7) | 253.0 ± 14.7 (240.3 – 271.4) |
| HA | 17.1 ± 3.3 (11.7- 20.3) | 28.8 ± 5.5 (19.9 – 34.9) | 290.2 ± 75.7 (216.4 – 411.9) |
| OM | 18.6 ± 2.0 (15.9 – 20.6) | 28.5 ± 9.6 (19.7 – 43.6) | 351.2 ± 125.5 (206.2- 524.4) |
| OT | 22.1 ± 3.5 (17.6 – 26.5) | 33.5 ± 4.5 (25.8- 37.1) | 384.7 ± 71.1 (292.7 – 490.3) |
| MA | 19.8 ± 3.3 (16.4 – 24.2) | 30.1 ± 9.7 (23.1 – 47.8) | 444.7 ± 205.4 (298.3 – 789.1) |
| ME | 19.5 ± 1.7 (17.3 – 22.0) | 23.7 ± 6.74 (15.2 – 31.6) | 274.1 ± 25.4 (151.5 – 282.6) |
| OE | 22.1 ± 4.4 (18.2 – 29.8) | 43.7 ± 12.8 (29.8 – 58.3) | 543.5 ± 169.3 (371.1 – 819.6) |
| **Average of all Samples** | **20.5 ± 3.5 (11.7 – 29.8)** | **31.4 ± 8.9 (15.2 – 58.3)** | **350.6 ± 124.6 (206.2 – 819.6)** |
| **UNCEAR2000 (average)** | **35.0** | **30.0** | **400.0** |

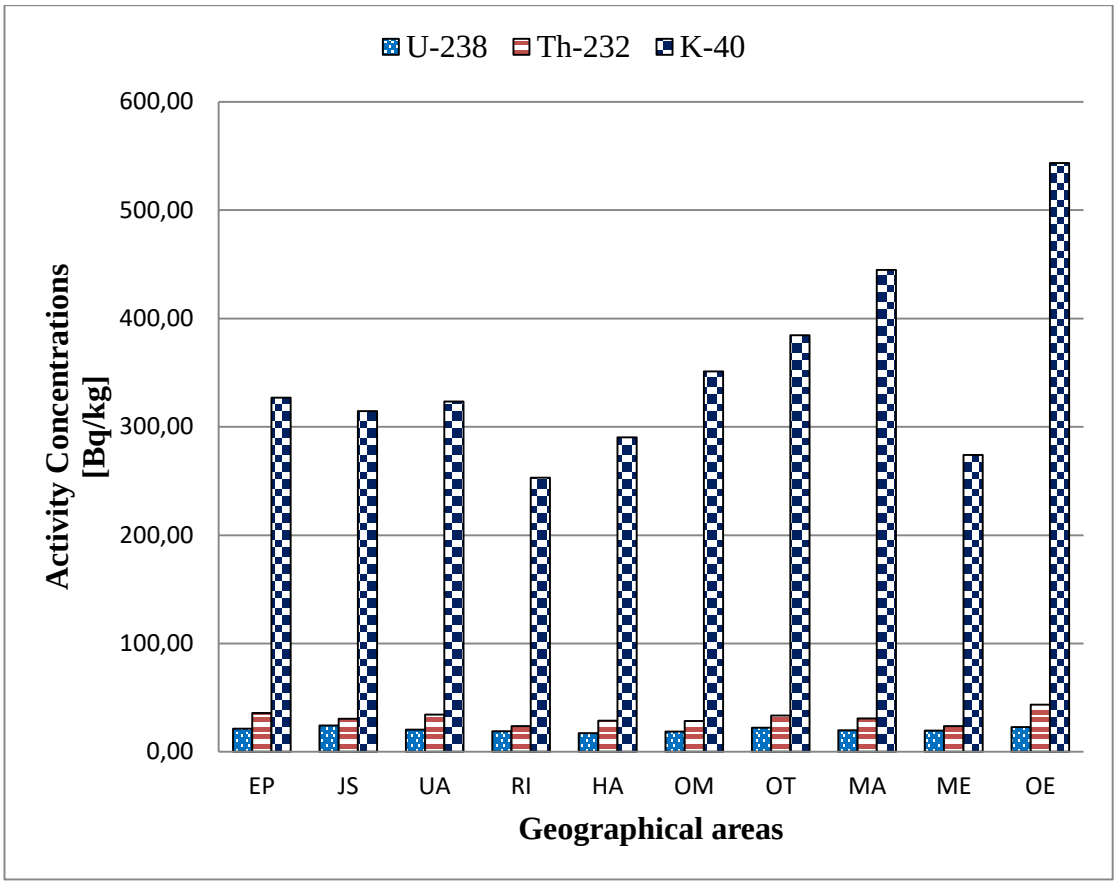


Figure 4.1: The mean activity concentrations of $^{238}U$, $^{232}Th$, and $^{40}K$ in the ten geographical areas of Outjo.

### 4.1.1 Statistical analysis of the activity concentrations of $^{238}U$, $^{232}Th$ and $^{40}K$

Table 4.2: Descriptive statistics of the results obtained in the measurements of radionuclide concentrations in the soil of Outjo

| Descriptive Statistics | $^{238}U$ conc (Bq $kg^{-1}$) | $^{232}Th$ conc (Bq $kg^{-1}$) | $^{40}K$ Conc (Bq $kg^{-1}$) |
|---|---|---|---|
| min | 11.7 | 15.2 | 206.2 |
| max | 29.8 | 58.3 | 819.6 |
| range | 18.0 | 43.1 | 613.5 |
| mean | 20.5 | 31.4 | 350.6 |
| standard deviation | 3.5 | 8.9 | 124.6 |
| standard error | 0.5 | 1.2 | 17.4 |
| median | 20.1 | 30.7 | 312.1 |
| skew | 0.4 | 0.9 | 2.1 |
| kurtosis | 0.6 | 1.1 | 5.6 |
| Number of samples | 50 | 50 | 50 |

Figure 4.2 shows the frequency distributions of activity concentrations of (a) $^{238}U$, (b) $^{232}Th$ and (c) $^{40}K$ in the soil samples collected across Outjo. As observed in Table 4.2 (column 2) and Figure 4.2(a), the concentrations of $^{238}U$ have almost a normal distribution with a skewness of 0.4 which is positive. Skewness is the degree of symmetry of the distribution. This means that the frequency curve of the distribution has a longer tail to the right of the central maximum than to the left. If the reverse of the latter is true, then the distribution is said to have a negative skew. The concentration of $^{238}U$ in most of the samples is between 15 Bq $kg^{-1}$ and 30 Bq $kg^{-1}$. In Figure 4.2 (a),

none of the fifty samples had an activity concentration greater than 30 Bq $kg^{-1}$. The most frequently occurring range of activity concentration of $^{238}U$ is 19 Bq $kg^{-1}$ to 20 Bq $kg^{-1}$. As shown in Figure 4.2 (b), the activity concentration of $^{232}Th$ in the samples have almost a normal distribution with a skewness of 0.9. Also, the concentration of $^{232}Th$ in most of the samples is between 19 Bq $kg^{-1}$ and 50 Bq $kg^{-1}$ and only two samples have an activity concentration greater than 50 Bq $kg^{-1}$while only one sample has an activity concentration less than 19 Bq $kg^{-1}$. There two most frequently occurring range of $^{232}Th$. These are 27 – 30 Bq $kg^{-1}$ and 35 – 38 Bq $kg^{-1}$. Similarly, the activity concentrations of $^{40}K$ in the samples have almost a normal distribution with a skewness of 2.1. In Figure 4.2 (c), the concentration of $^{40}K$ in most of the samples is between 206 Bq $kg^{-1}$ and 631 Bq $kg^{-1}$ and only two samples have an activity concentrations greater than 631 Bq $kg^{-1}$. None of the samples has an activity concentration less than 206 Bq $kg^{-1}$ and the most frequently occurring range of activity concentration of $^{40}K$ is 267 Bq $kg^{-1}$ to 327 Bq $kg^{-1}$.

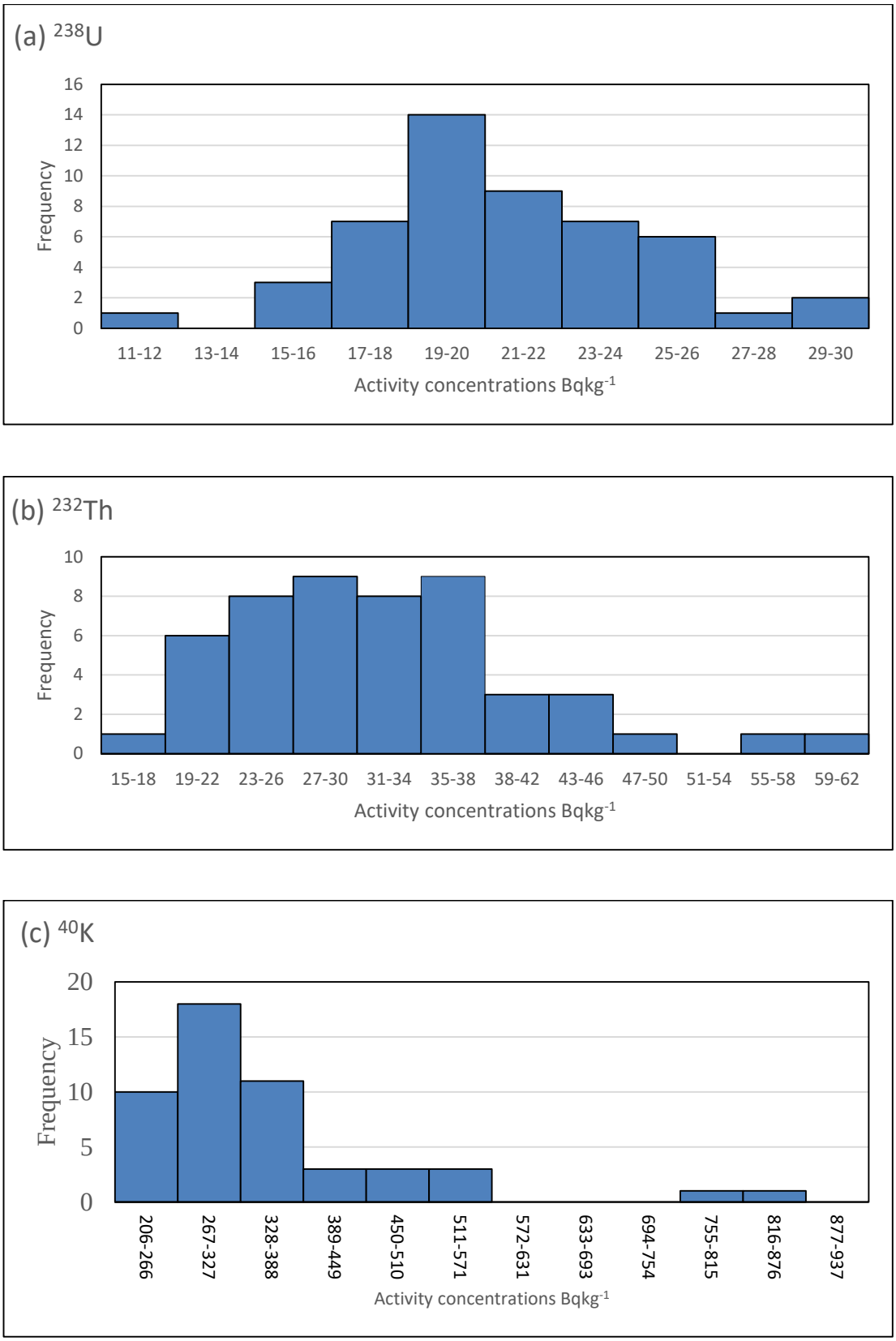


Figure 4.2: Frequency distributions of the concentrations of (a) $^{238}U$, (b) $^{232}Th$, and (c) $^{40}K$ in the soil of Outjo.

### 4.1.2 Correlation studies for the activity concentrations

The linear correlation coefficient was used to establish a correlation between pairs of different radionuclides. A correlation is a numerical measure to describe the degree of strength and direction by which one variable is related to another. The correlation coefficient can range in value between -1 to +1 [67]. A positive correlation implies that there is a direct relationship between the variables while a negative correlation indicates an inverse relationship. Figure 4.3 shows the correlation analysis of the values of the activity concentrations of $^{238}U$, $^{232}Th$ and $^{40}K$ in the soils of Outjo. As could be observed in Figure 4.3, there exists a positive correlation of 0.34 between $^{238}U$ and $^{232}Th$, 0.19 between $^{238}U$ and $^{40}K$ and 0.64 between $^{232}Th$ and $^{40}K$. Furthermore, the correlation plots in Figure 4.3 (a) and (b) shows a weak relationship between $^{238}U$ and $^{232}Th$ and between $^{238}U$ and $^{40}K$ respectively. In contrast, there is a strong correlation of 0.64 between $^{232}Th$ and $^{40}K$.

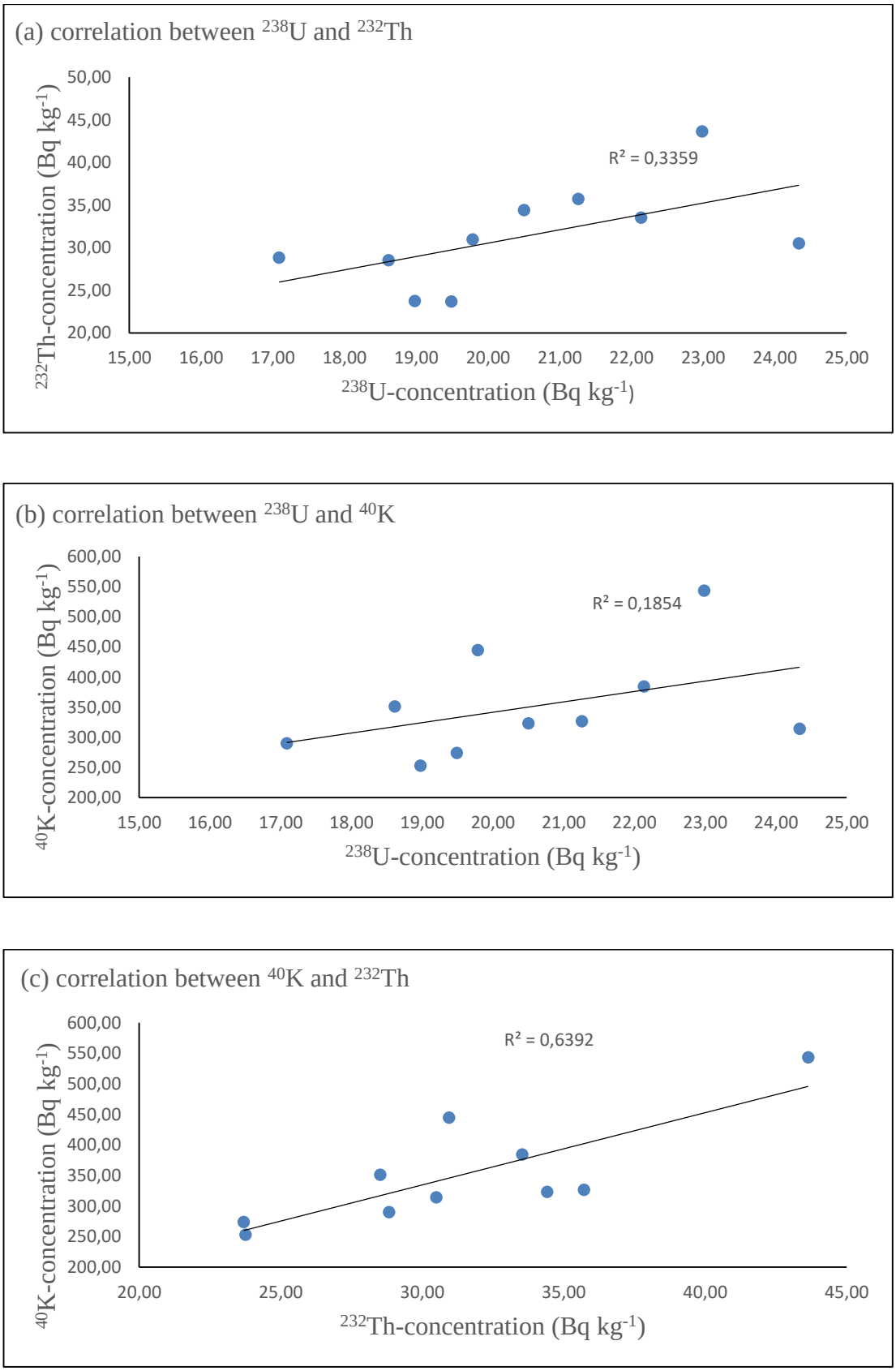


Figure 4.3: The correlation between the activity concentrations of (a) $^{238}U$ and $^{232}Th$, (b) $^{238}U$ and $^{40}K$ and (c) $^{232}Th$ and $^{40}K$.

### 4.1.3 Comparison of the average activity concentrations of $^{238}U$, $^{232}Th$ and $^{40}K$ in the soil of Outjo with those measured in the soils of some other towns in Namibia

Figure 4.4 summarizes the results of the comparison of the mean activity concentrations in the town of Outjo with those obtained in some other towns in Namibia. The towns are Usakos, Arandis, Swakopmund, Walvis Bay, Tsumeb, Oshakati, Rundu and Katima Mulilo. In Figure 4.4, the soil samples from Outjo contain lower activity concentrations of $^{238}U$ and $^{232}Th$ than Usakos, Arandis and Swakopmund. Also, the concentration of $^{40}K$ in the soil of the town of Outjo is lower than that of Usakos, Arandis, Swakopmund, Walvis Bay and Tsumeb. Consequently, the mean activity concentration for $^{238}U$, $^{232}Th$ and $^{40}K$ in the town of Outjo is higher than in Oshakati, Rundu, and Katima Mulilo. With the exemption of Oshakati, Rundu, Katima Mulilo and Walvis Bay, the average activity concentrations of $^{238}U$, $^{232}Th$ and $^{40}K$ in the other towns are much higher than the worldwide average activity concentrations of 35 Bq $kg^{-1}$, 30 Bq $kg^{-1}$ and 400 Bq $kg^{-1}$ for $^{238}U$, $^{232}Th$ and $^{40}K$ respectively [23] .

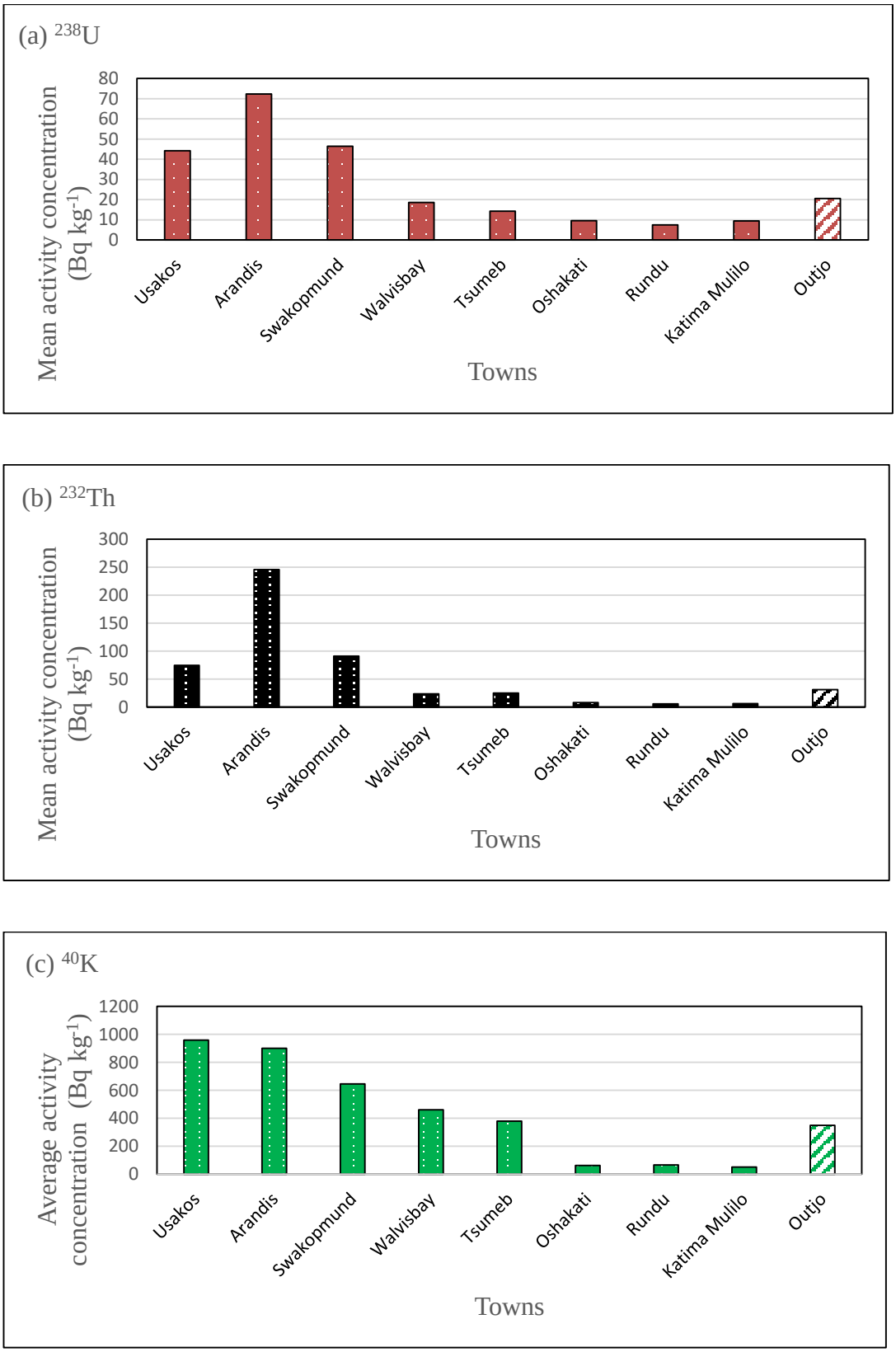


Figure 4.4: Comparison of the mean activity concentrations of (a) $^{238}U$,(b) $^{232}Th$ and (c) $^{40}K$ in the soil of Outjo with those of some other towns in Namibia.

## 4.2 Assessment of radiological hazard

### 4.2.1 Radiation absorbed dose and the annual effective dose

The absorbed dose rates in the air at 1 m above the ground were calculated using the values obtained for the activity concentrations of $^{238}U$, $^{232}Th$ and $^{40}K$ in the soil samples of Outjo. In Table 4.3 (column 2), the absorbed dose rates in Outjo varies from 27.6 ± 1.5 $nGyh^{-1}$ in the ME area to 83.2 ± 3.0 $nGyh^{-1}$ in the OE area with an average value of 43.0 ± 10.6 $nGyh^{-1}$. Figure 4.5 (a) shows the mean absorbed dose rates for the ten geographical areas of Outjo. The average value obtained for the absorbed dose rate is less than the worldwide average outdoor value of 58 $nGyh^{-1}$ reported for normal background areas.

The annual effective dose for each area was calculated (using equation 3.7) from the corresponding absorbed dose rate. In Table 4.3 (column 3), the annual effective dose varies from 0.03 mSv (in the ME) to 0.10 mSv (in the OE) with a mean value of 0.05 ± 0.01 mSv. In Figure 4.5 (b), the mean values of the effective dose rate are below the maximum permissible limit of 1.00 mSv recommended by the International Commission on Radiological Protection (ICRP). This implies that the background radiation in the town is not high.

Table 4.3: Mean absorbed dose rate and average annual effective dose in different geographical areas of Outjo. The range of values in each geographical area is given in parenthesis.

| **Area** | **Absorbed dose rate ($nGyh^{-1}$)** | **Annual effective dose (mSv)** |
|---|---|---|
| EP | 45.0 ± 8.5<br>(30.3 – 51.2) | 0.06 ± 0.01<br>(0.04 – 0.06) |
| JS | 42.8 ± 6.0<br>(33.9 – 50.5) | 0.05 ± 0.01<br>(0.04 – 0.06) |
| UA | 43.7 ± 3.6<br>(41.6 – 50.1) | 0.05 ± 0.00<br>(0.05 – 0.06) |
| RI | 33.7 ± 2.5<br>(31.6 – 36.4) | 0.04 ± 0.00<br>(0.04 – 0.05) |
| HA | 37.4 ± 6.9<br>(28.3 – 47.2) | 0.05 ± 0.01<br>(0.04 – 0.06) |
| OM | 40.5 ± 10.8<br>(31.3 – 53.7) | 0.05 ± 0.01<br>(0.04 - 0.07) |
| OT | 46.5 ± 5.4<br>(37.2 – 50.4) | 0.06 ± 0.01<br>(0.05 – 0.06) |
| MA | 46.4 ± 11.6<br>(34.9 – 60.0) | 0.06 ± 0.01<br>(0.04 – 0.07) |
| ME | 34.74 ± 5.54<br>(27.6 – 40.10) | 0.04 ± 0.01<br>(0.03 – 0.05) |
| OE | 59.10 ± 16.2<br>(43.5 – 83.2) | 0.07 ± 0.02<br>(0.05 – 0.10) |
| **Average of all samples** | **43.0 ± 10.6<br>(27.6 – 83.2)** | **0.05 ± 0.01<br>(0.03 -0.10)** |

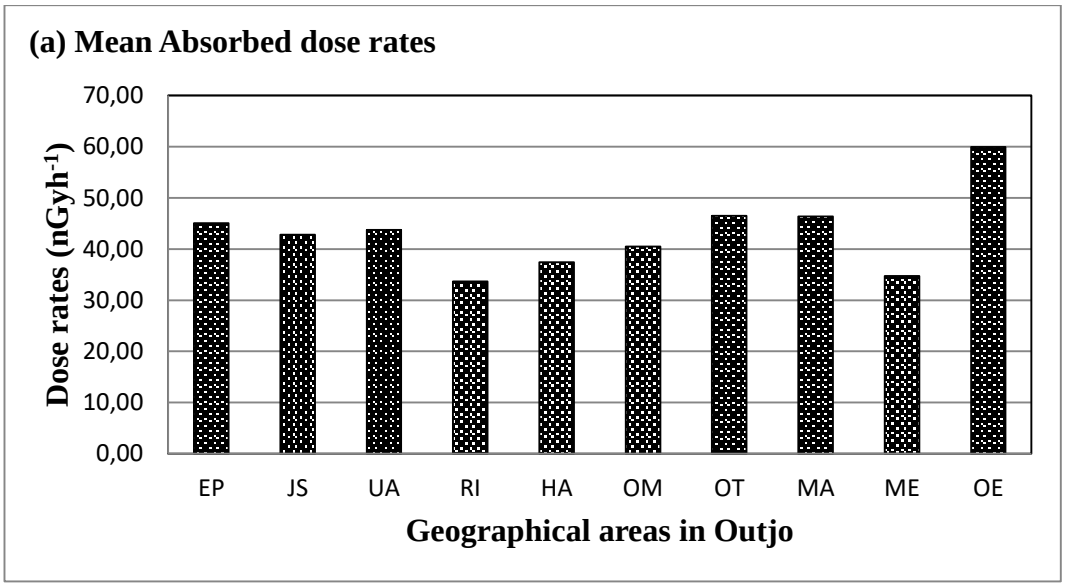


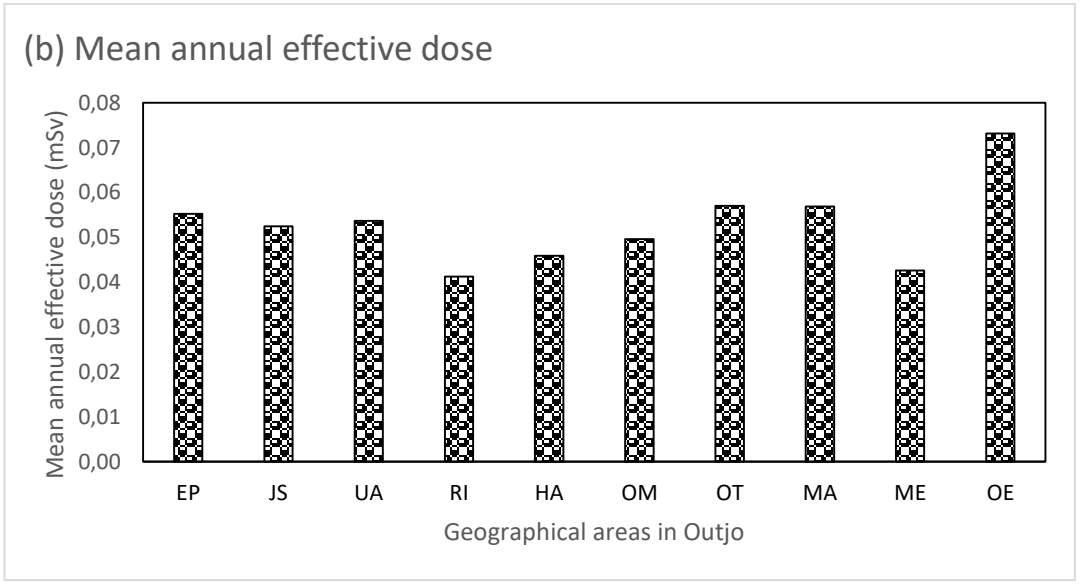


Figure 4.5: The mean (a) absorbed dose rates and (b) the effective dose rates in the ten geographical areas of Outjo.

Figure 4.6 shows the frequency distribution of the (a) absorbed dose rates and (b) annual effective dose in all the ten geographical areas of Outjo. The absorbed dose rates have a frequency distribution with a skewness of 1.3 and kurtosis of 3.1. In Figure 4.6 (a), most of the absorbed dose rates calculated are between 27 $nGyh^{-1}$ and 68 $nGyh^{-1}$. Only one of the absorbed dose rates is greater than 68 $nGyh^{-1}$ and the most frequently

occurring range of absorbed dose rates is from 33 $nGyh^{-1}$ to 38 $nGyh^{-1}$. Also, the most frequently occurring ranges of effective dose rates are from 0.037 $mSvy^{-1}$ to 0.043 $mSvy^{-1}$ and 0.051 $mSvy^{-1}$ to 0.057 $mSvy^{-1}$ as shown in Figure 4.6 (b). Most of the effective doses are between 0.03 $mSvy^{-1}$ and 0.08 $mSvy^{-1}$ and only one sample has an effective dose rate greater than 0.085$mSvy^{-1}$.

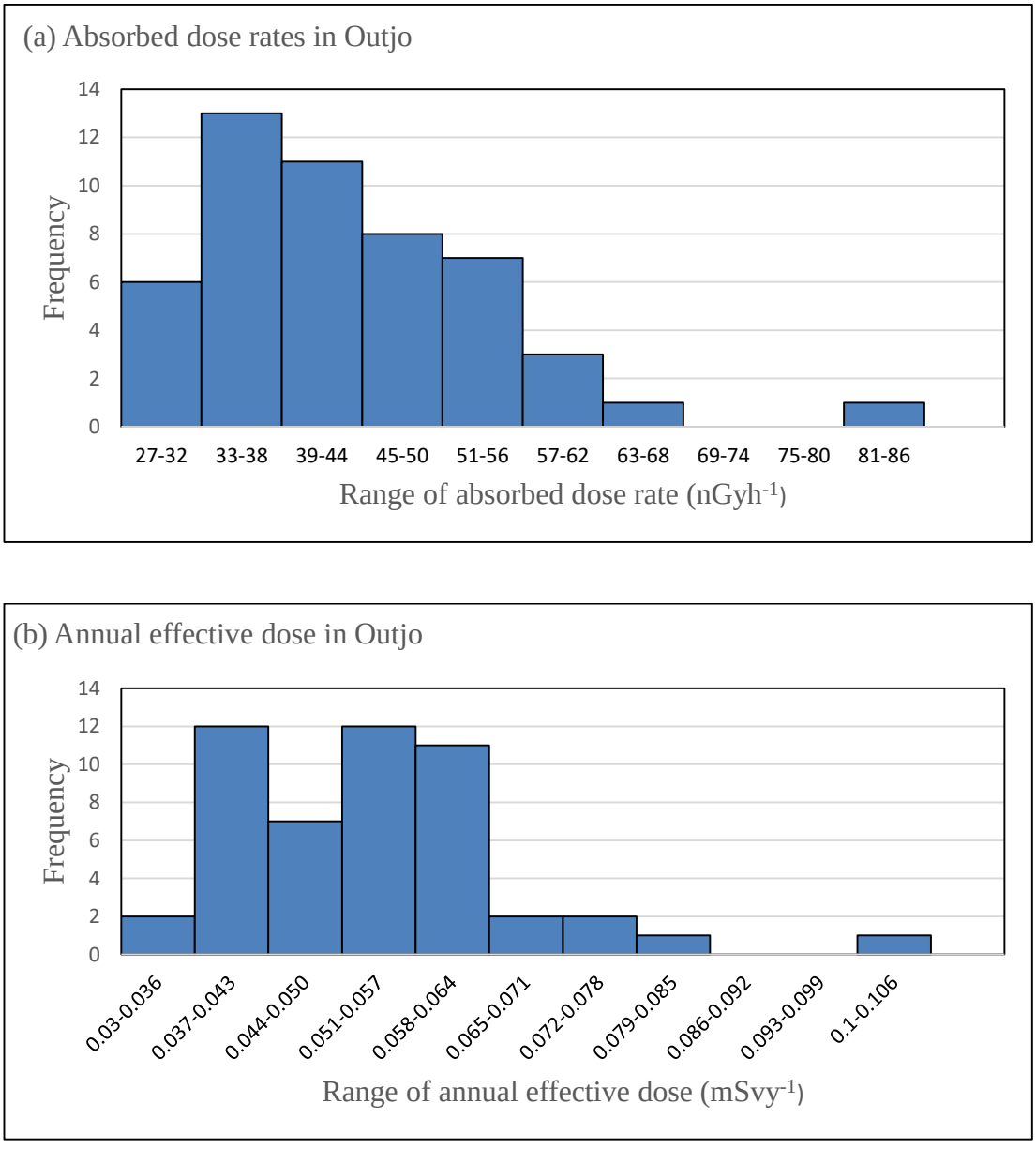


Figure 4.6: Frequency distributions of (a) absorbed dose rates and (b) annual effective dose in Outjo.

### 4.2.2 Radium equivalent activity

The average Radium equivalent activity in the ten geographical areas of Outjo is presented in Table 4.4 and shown in Figure 4.7. In Table 4.4 and Figure 4.7, the Radium equivalent activity is in the range 58.3 ± 3.3 Bq $kg^{-1}$ to 176.3 ± 6.8 Bq $kg^{-1}$. The ME area has the lowest Radium equivalent activity while the OE area has the highest. The average Radium equivalent activity from all ten geographical areas in Outjo is 92. 4 ± 22.5 Bq $kg^{-1}$. This value is below the recommended maximum of 370 Bq $kg^{-1}$.

Table 4.4: The average Radium equivalent activity in different geographical areas of Outjo. The range of values is given in parenthesis.

| **Area** | **Radium equivalent activity ($R_{aeq}$) [Bq/kg]** |
|---|---|
| EP | 97.5 ± 19.3<br>(64.8 – 111.3) |
| JS | 92.2 ± 13.0<br>(72.8 – 108.5) |
| UA | 94.6 ± 7.6<br>(90.0 – 108.2) |
| RI | 72.4 ± 5.4<br>(67.7 – 78.3) |
| HA | 80.7 ± 14.7<br>(60.3 – 100.9) |
| OM | 86.4 ± 23.0<br>(67.9 – 115.8) |
| OT | 99.7 ± 11.5<br>(79.7 – 108.6) |
| MA | 98.3 ± 24.0<br>(74.2 – 129.5) |
| ME | 74.5± 12.5<br>(58.3 - 88.4) |
| OE | 127.3 ± 34.5<br>(93.3 – 176.3) |
| **Average of all samples** | **92.4 ± 22.5**<br>**(58.3 – 176.3)** |

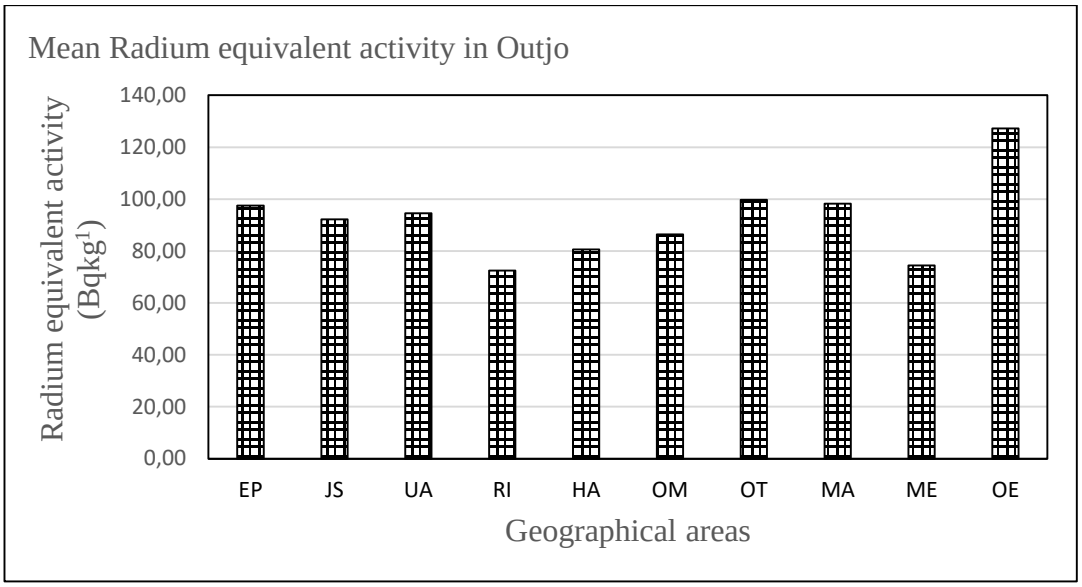


Figure 4.7: The mean Radium equivalent activity in the ten geographical areas of Outjo.

The frequency distribution of Radium equivalent activities is shown in Figure 4.8. As could be observed in Figure 4.8, most of the Radium equivalent activities calculated for the samples are between 58 Bq $kg^{-1}$ and 153 Bq $kg^{-1}$ and only one Radium equivalent activity is greater than 153 Bq $kg^{-1}$. Also, the most frequently occurring range of Radium equivalent activity is from 82 Bq $kg^{-1}$ to 93 Bq $kg^{-1}$.

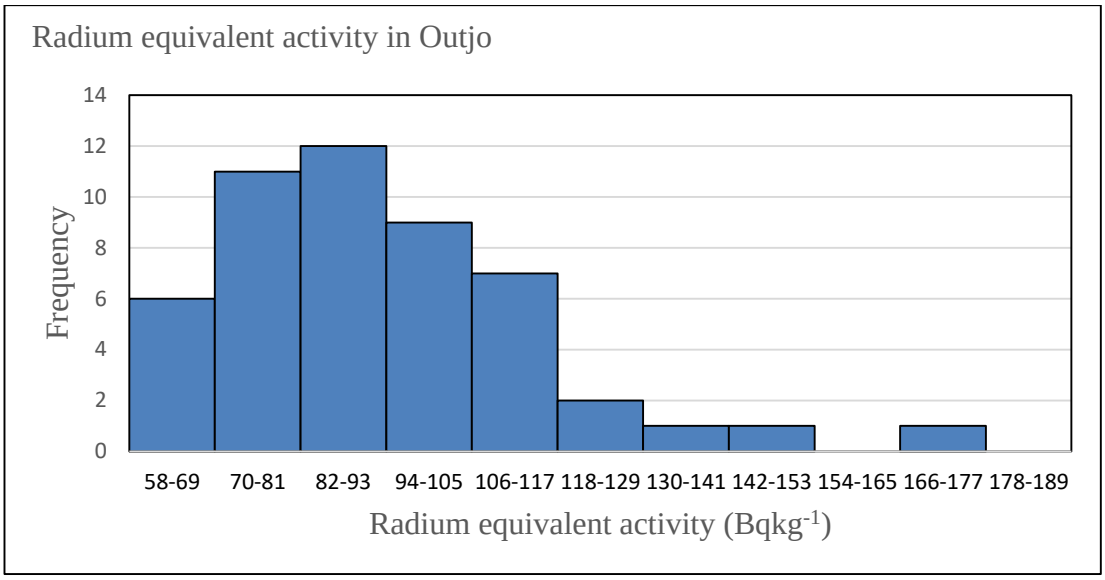


Figure 4.8: Frequency distribution of Radium equivalent activity in Outjo

### 4.2.3 Internal ($H_{in}$) and External ($H_{ex}$) hazard indices

The internal hazard indices in the soil samples ranged from 0.19 ± 0.01 in the HA area to 0.56 ± 0.02 in the OE area as presented in Table 4.5 (column 2). The mean internal hazard index in the town of Outjo is 0.30 ± 0.07. In Figure 4.9 (a), the RI and ME areas have the lowest mean internal hazard indices while the OE area has the highest index. Similarly in Table 4.5 (column 3), the external hazard index is in the range of 0.16 ± 0.01 to 0.48 ± 0.02 with the lowest in the ME area and the highest in the OE area. Also, the average external hazard index in all the ten geographical areas is 0.25 ± 0.06. These mean values are less than 1, and implies that radiation hazard is negligible in the town.

Table 4.5*:* The mean internal and external hazard indices in Outjo.

| **Area** | **Internal hazard index ($H_{in}$)** | **External hazard index ($H_{ex}$)** |
|---|---|---|
| EP | 0.32 ± 0.06 (0.22 – 0.37) | 0.26 ± 0.05 (0.18 – 0.30) |
| JS | 0.31 ± 0.04 (0.26 – 0.37) | 0.25 ± 0.04 (0.20 – 0.29) |
| UA | 0.31 ± 0.02 (0.30 – 0.35) | 0.26 ± 0.02 (0.24 – 0.21) |
| RI | 0.25 ± 0.02 (0.23 0.27) | 0.20 ± 0.01 (0.18 – 0.21) |
| HA | 0.26 ± 0.05 (0.19 – 0.32) | 0.22 ± 0.04 (0.16 – 0.27) |
| OM | 0.28 ± 0.07 (0.23 – 0.37 ) | 0.23 ± 0.06 (0.18 – 0.31) |
| OT | 0.33 ± 0.04 (0.27 – 0.36) | 0.27± 0.03 (0.22 – 0.29) |
| MA | 0.32 ± 0.07 (0.25 – 0.42) | 0.27± 0.06 (0.20 – 0.35) |
| ME | 0.25 ± 0.04 (0.20 – 0.29) | 0.20 ± 0.03 (0.16 – 0.24) |
| OE | 0.41 ± 0.10 (0.30 – 0.56) | 0.34 ± 0.09 (0.25 – 0.48) |
| **Average of all samples** | **0.30 ± 0. 07 (0.19 – 0.56)** | **0.25 ± 0.06 (0.16 – 0.48)** |

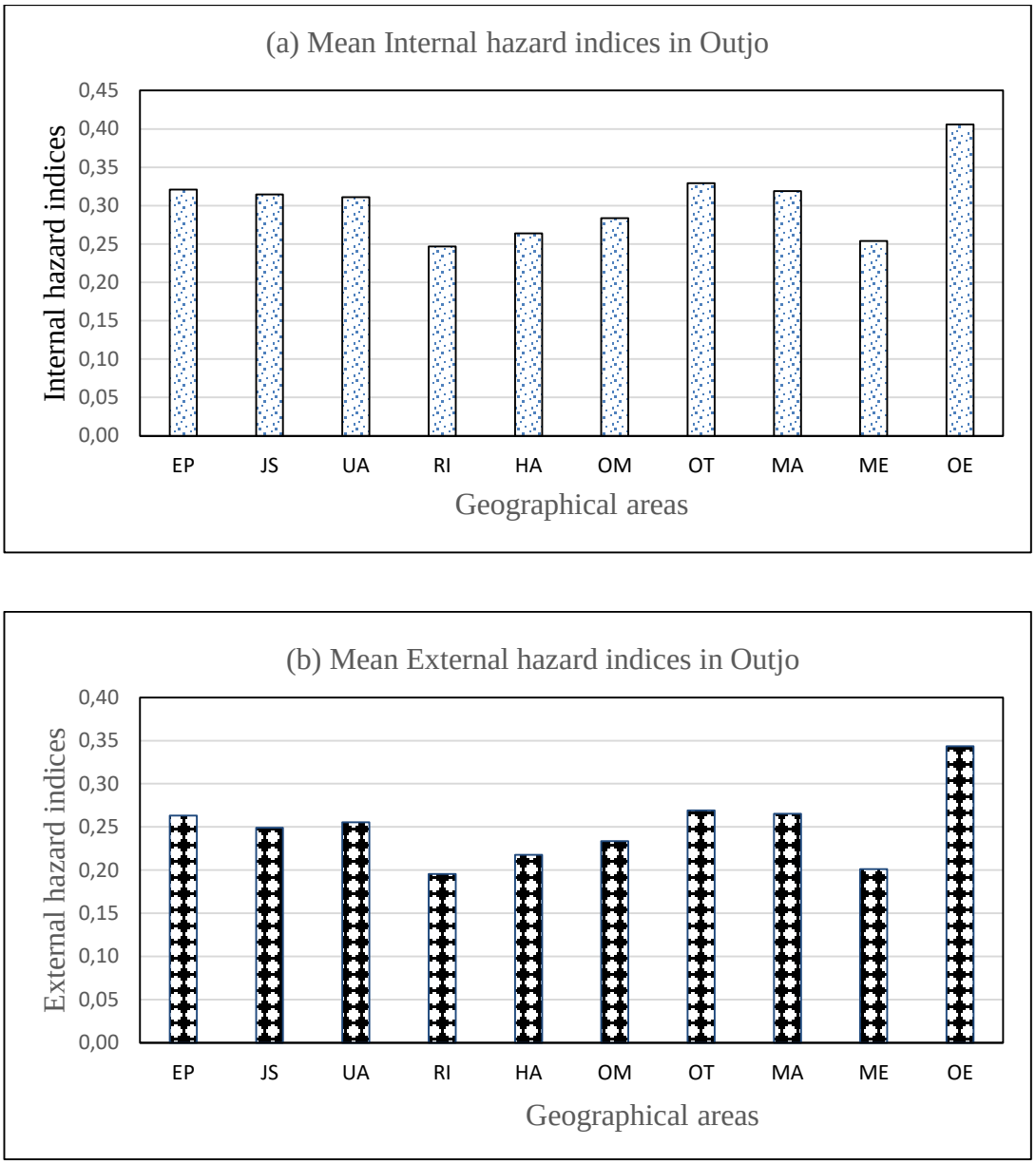


Figure 4.9: The mean (a) Internal hazard indices and (b) External hazard indices in the ten geographical areas of Outjo.

Figure 4.10 show the frequency distribution of (a) internal hazard indices and (b) external hazard indices in all the ten geographical areas of Outjo. Figure 4.10 (a) illustrates internal hazard indices between 0.23 and 0.34. Only one of the indices are above 0.34. Similarly, most of the External hazard indices calculated for the samples are between 0.16 and 0.43 as shown in Figure 4.10 (b). Only one of the external hazard

indices is greater than 0.43 and the most frequently occurring range of External hazard index is between 0.25 and 0.28. These low values again confirm that radiation hazard is negligible in the town of Outjo.

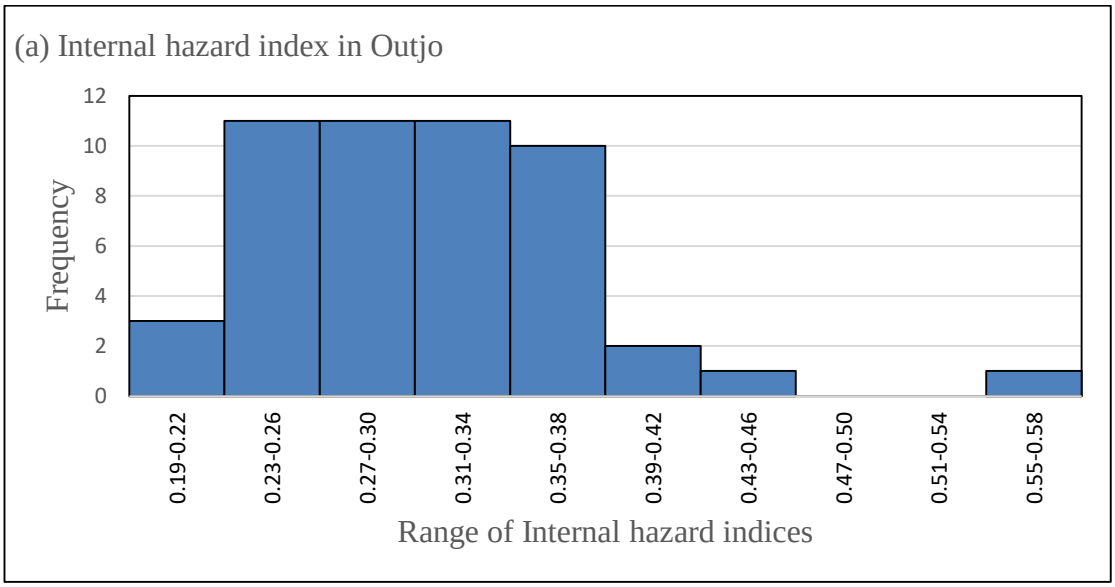


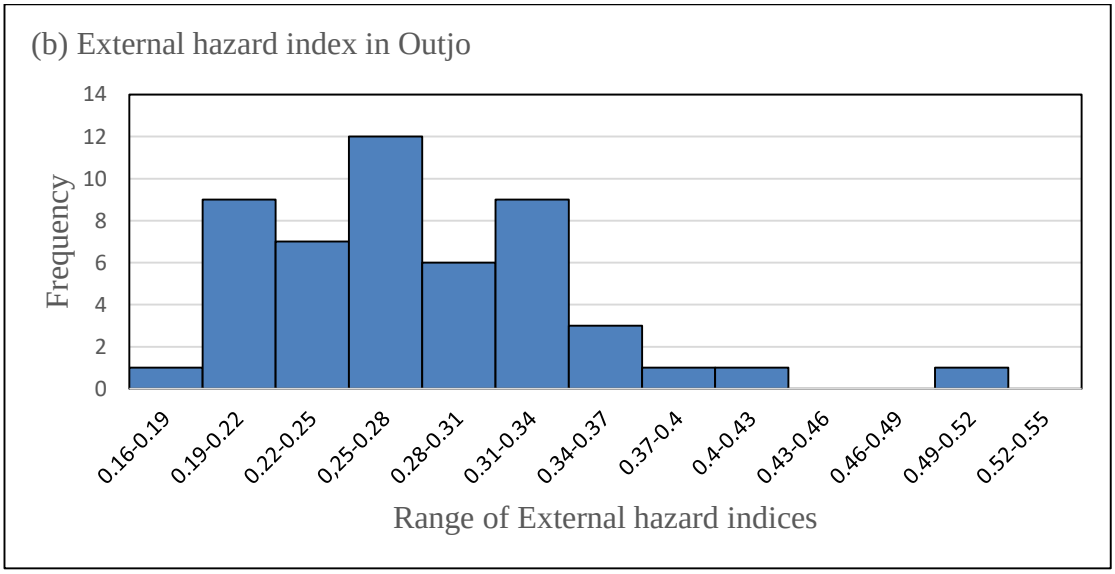


Figure 4.10: Frequency distributions of (a) Internal and (b) External hazard indices in the soil samples of Outjo.

### 4.2.4 Gamma index ($I_\gamma$) in the town of Outjo

The mean values of gamma index obtained from the activity concentrations of uranium, thorium and potassium are presented in Table 4.6 and shown in Figure 4.11. The gamma index ranged from 0.22 ± 0.01 to 0.66 ± 0.02 with the mean value of 0.34 ± 0.09. Figure 4.11 indicates that the RI and ME areas have the lowest mean gamma index while the OE area has the highest gamma index .The mean gamma index in the town of Outjo is less than unity, hence the radiation hazard in the town is negligible.

Table 4.6: Average gamma indices in the ten geographical areas of Outjo. The corresponding range of values is given in parentheses.

| **Area** | **Gamma index ($I_\gamma$)** |
|---|---|
| EP | 0.36 ± 0.07<br>(0.24 – 0.41) |
| JS | 0.34 ± 0.05<br>(0.27 – 0.40 ) |
| UA | 0.35 ± 0.03<br>(0.33 - 0.40) |
| RI | 0.27 ± 0.02<br>(0.25 – 0.29) |
| HA | 0.30 ± 0.05<br>(0.23 – 0.38) |
| OM | 0.32 ± 0.09<br>(0.25 – 0.43) |
| OT | 0.37 ± 0.04<br>(0.29 – 0.40) |
| MA | 0.37 ± 0.09<br>(0.28 - 0.48) |
| ME | 0.27 ± 0.04<br>(0.22 – 0.33) |
| OE | 0.48 ± 0.13<br>(0.35 – 0.66) |
| **Average of all samples** | **0.34 ± 0.09**<br>**(0.22 – 0.66)** |

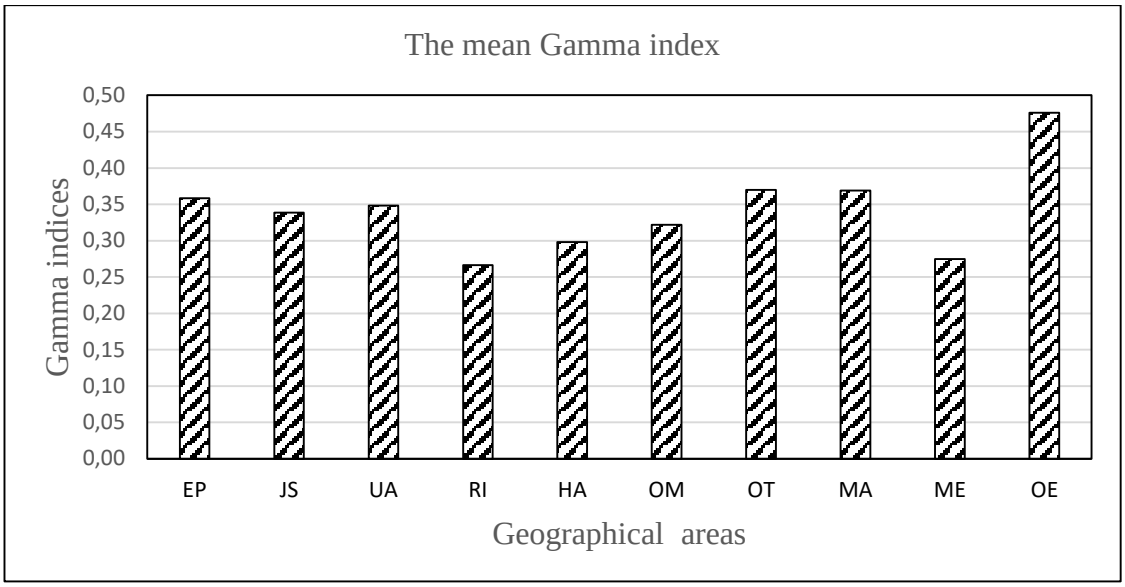


Figure 4.11: The mean Gamma index in the ten Geographical areas of Outjo

The frequency distribution of gamma index is shown in Figure 4.12. In Figure 4.12, most of the gamma indices calculated for the samples are between 0.22 and 0.41. Only six indices are above 0.41 and the most frequently calculated gamma indices are between 0.32 and 0.36.

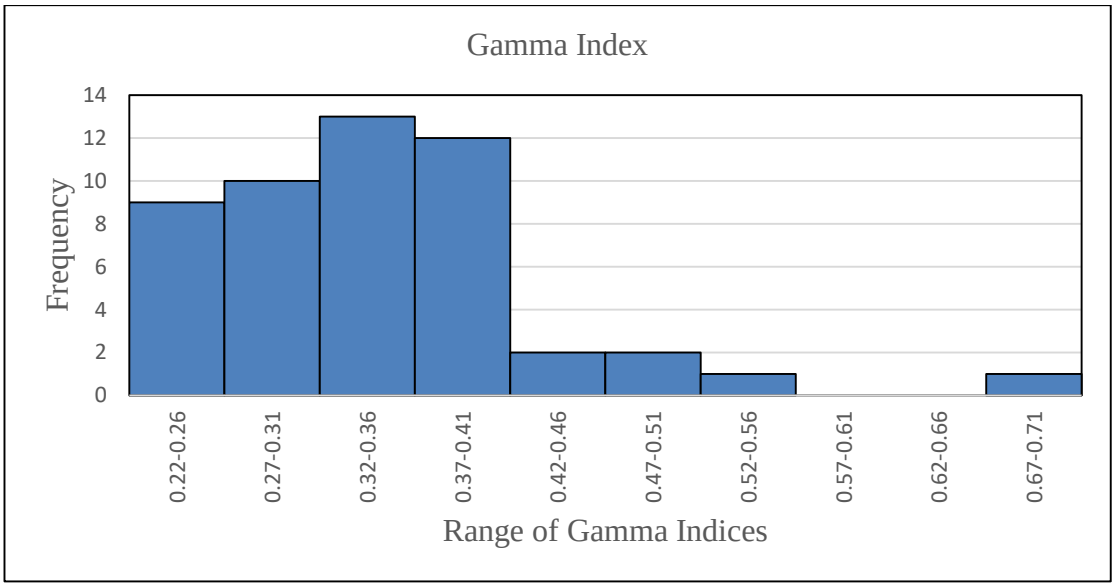


Figure 4.12: Frequency distribution of gamma indices in the soil samples of Outjo.

# CHAPTER 5

# 5 CONCLUSIONS AND RECOMMENDATIONS

## 5.1 Conclusion

The activity concentrations of $^{238}U$, $^{232}Th$ and $^{40}K$ in 50 soil samples collected from across the town of Outjo were determined by gamma spectroscopy. The mean activity concentrations of $^{238}U$ is 20.5 ± 3.5 Bq $kg^{-1}$ while that of $^{232}Th$ is 31.4 ± 8.9 Bq $kg^{-1}$ and for $^{40}K$ is 350.6 ± 124.6 Bq $kg^{-1}$ respectively. These concentrations with the exception of $^{232}Th$ are lower than the worldwide average values. In contrast, the average activity concentration for $^{232}Th$ is slightly higher than the worldwide average of 30.0 Bq $kg^{-1}$.

The radiological hazards associated with the radionuclides in the soils collected from the ten geographical areas of Outjo were calculated. The average absorbed dose rate is lower than the worldwide average value and the effective dose rate is below the maximum permissible limit. These results implies that the town does not have a high background radiation. Also, the values obtained for $Ra_{eq}$ and other hazard indices such as $H_{in}$, $H_{ex}$ and $I_{\gamma}$ are all below their corresponding maximum permissible limits. These results further confirm that the town of Outjo has a normal background radiation.

## 5.2 Recommendations and suggestions for further work

Further studies should be carried out to determine the levels of activity concentrations of naturally occurring radionuclides in ground water, marine ecosystem and plants in the town of Outjo. Studies to estimate the doses due to Radon ($^{222}Rn$) gas and its decay products should also be carried out. Also, studies on radiation exposure due to building materials in Outjo can be conducted and this study can also be extended to other towns

especially those with mineral resources such as Otjiwarongo, Otavi, Rosh Pinah and Orangemund in Namibia.

**REFERENCES**

[1] G. F. Knoll, Radiation Detection and Measurements, 3rd ed., New York: John Willey & Sons Inc, 2000.

[2] A. S. Shimboyo, "Natural radioactivty in soils of the Walvis Bay-Henties Bay Coastal area Namibia," *International Science and Technology Journal of Namibia (ISTJN),* vol. 5, pp. 104-110, 2013.

[3] L. N. Raymond, M. T. Victor, A. K. Nnenesi and Z. Munyaradzi, "Hazards Index Analysis of Gamma Emitting Radionuclides in Selected Areas Around the Uranium Mine Sites at Erongo Region, Namibia," *Journal of Environmental Science and Management,* vol. 19, no. 2, pp. 1-7, December 2016.

[4] S. Shimboyo, J. Oyedele and S. Sitoka, "Soil Radioactivity Levels And Associated Hazards In Selected Towns In Uranium-Rich Western Namibia," *International Science and Technology Journal of Namibia (ISTJN),* vol. 7, pp. 73-84, 06 April 2016.

[5] K. Tibor, S. Gabor, F. Ferenc, K. Richard and A. Gregoric, "Systematic Survey of natural radioactivity of soil in Slovenia," *Journal of Environmental Radioactivity,* vol. 122, no. 2013, pp. 70-78, 1 April 2013.

[6] J. A. Oyedele, "Assesment of the natural radioactivity in the soils of Windhoek city,Namibia,Southern Africa," *Radiation Protection Dosimetry,* pp. 337-340, 28 February 2006.

[7] G. Shanthi, T. K. Thampi, G. R. Allen and C. G. Maniyan, “Measurement of activity concentration of natural radionuclides for the assesment of radiological indices,” *Radiation Protection Dosimetry,* no. 2010, pp. 1-7, 23 April 2010.

[8] H. H. Jolyon, S. L. Steven, W. Andrzej, S. Mehdi, B. Werner, C. Elisabeth, L. Dominique, T. Margot and H. Isamu, “Human exposure to high natural background radiation: what can it teach us about radiation risks?,” *Journal of Radiological Protection,* vol. 29, no. 2A, 19 May 2009.

[9] S. Mujahid and S. Hussain, “Natural Radioactivity in soil in the Baluchistan province of Pakistan,” *Radiation Protection Dosimetry,* vol. 140, no. 4, pp. 333-339, 26 April 2010.

[10] H. Shindondola-Mote, “Uranium mining in Namibia, "The mystery behind low level radiation",” 2008.

[11] J. Oyedele, S. Sitoka and I. Davids, “Radionuclide Concentrations in soils of northern Namibia,Southern Africa,” *Radiation Protection Dosimetry,* vol. 131, no. 4, pp. 482-486, 22 July 2008.

[12] C. Giancoli, Physics, New Jersey: Prentice Hall International Inc, 1998.

[13] J. Oyedele, Nuclear Physics, Centre for External Sturdies, University Of Namibia-Windhoek,Namibia, 2012.

[14] A. Allisy, “Henry Becquerel: The Discovery of Radioactivity,” *Radiation Protection Dosimetry,* vol. 68, no. 1-2, pp. 3-10, 01 November 1996.

[15] D. Shahbazi-Gahrouei, M. Gholami and S. S. Setayandeh, “A review on natural background radiation,” *Advanced Biomedical Research,* vol. 2, no. 65, 2013.

[16] P. M. Katse, “Determination of Natural Radioactivity Concentrations in Soil: a comparative study of Windows and Full Spectrum Analysis,” 2004.

[17] K. S. Kenneth, Introductory Nuclear Physics, New York: John Willey & Sons, 1988.

[18] United Nations Scientific Comitee on the Effets of Atomic Radiation (UNSCEAR), “Sources and effects of ionizing radiation,” United Nations Publications, New York, 2008.

[19] E. E. Taapopi, A. Faanu and S. Dampare, “Assesment of naturally occuring radioactive materials and trace elements in playgrounds of selected basic schools in the GA east municipal district,Accra,Ghana,” *International Science and Technology Journal of Namibia (ISTJN),* vol. 10, no. 1, pp. 133 - 147, 23 OCctober 2017.

[20] J. S. Stanley, “Natural Radiation,” *Virginia Minerals,* vol. 37, no. 2, pp. 10-15, May 1991.

[21] N. Sighn, Radioisotopes-Applications in Phsical Science, Croatia: In Tech, 2011.

[22] Canadian Nuclear Safety Commision (CNSC), “Introduction to Radiation,” 2012.

[23] United Nations Scientific Commitee on the Effects of A tomic Radiation (UNSCEAR), “Sources and effects of ionizing radiation-Exposures from natural sources(annex b),” United Nations, New York, 2000.

[24] M. Wilfred, “An avaluation of the Natural Radioactivity in the soils of Okahandja and Karibib, Namibia.,” Windhoek, 2017.

[25] L. Michael, Handbook of Radioactivity Analysis, Elsevier Inc, 2012.

[26] A. Bouville and W. M. Lowdert, “Human Population Exposure to cosmic radiation,” *Radiation Protection Dosimetry,* vol. 24, no. 14, pp. 293 - 199, 1988.

[27] R. D. Evans, The Atomic Nucleus, Bombay-Nee Delhi: Tata McGRAIN-HILL, 1955.

[28] D. Ramesh, “Atomic Structure & Basic Concepts of Chemistry,” 18 April 2018.

[29] M. Roy, “Atoms, Molecules, Matter : The Stuff of Chemistry,” in *Basic books in science,* 2011, pp. 1-5.

[30] B. Bahr, B. Lemmer and R. Piccolo, “Alpha, Beta and gamma rays,” in *Quirky Quarks,* Berlin, Heidelberg, Springer, 2016, pp. 145-160.

[31] E. Boyes and M. Stanisstreet, “Children's Ideas about Radioactivity and Radiation: sources, mode of travel, uses and dangers,” *Research in Science & Technological Education,* vol. 12, no. 2, pp. 146-180, 01 January 1994.

[32] N. Kadhim, “lectures in Radiation Physics,” 2018.

[33] P. Cappellaro, “Introduction to applied nuclear physics,” Spring, 2012.

[34] D. N. Poenaru, Nuclear decay modes, Institute of Physics Publishing, Bristol ; Philadelphia, 1996.

[35] K. Heyde, Basic Ideas and Concepts in Nuclear Science: An Introductory Aproach, London: Institute Of Physics, 1999.

[36] International Atomic Energy Agency (IAEA), Radiation Biology: A Handbook for Teachers and Students, Viena: Viena International Centre, 2010.

[37] C. H. Arthur, "A Quantum Theory of the Scattering of X-rays by Light Elements," *The Physical Review,* vol. 21, no. 5, 1993.

[38] H. F. WIlliam, "The Interaction of Gamma Rays with Matter," *Pure and applied Physics,* vol. 9, no. Part A, pp. 211 - 227, 1960.

[39] V. K. Muraleedhara, Nuclear Radiation Detection: Measurements And Analysis, Oxford OX4 2JZ,UK: Alpha Science International LTD, 2009.

[40] T. Nicholas and L. Sheldon, Measurement and detection of Radiation, New york: Taylor & Francis Group, 2011.

[41] J. V. R. Theunis, "Radiation Protection and Health Physics," 2017.

[42] E. T. James, Atoms, Radiation and Radiation Protection, 3rd ed., Weinheim: Wiley-VCH Verlang GmbH & Co. KGaA, 2007.

[43] M. Rizzi, M. D'Aloia and B. Castagnol, "Semiconducgor detectors and principles of radiation-matter interaction," *Journal of Applied Science,* vol. 10, pp. 3141 - 3155, 2010.

[44] Canberra, “Germanium Detectors,” Mirion Technologies (Canberra), Inc, 2016.

[45] M. U. Khandaker, “High purity germanium detector in gamma-ray spectrometry,” *International Journal of Fundamental Physical Sciences,* vol. 1, no. 2, 2011.

[46] H. Börner and M. Jentschel, “High-resolution gamma-ray spectroscopy,” *Physics of Atomic Nuclei,* vol. 64, no. 6, pp. 1011 - 1014, 01 06 2001.

[47] J. Shapiro, Radiation Protection, 4th ed., Havard University Press, 2002.

[48] H. Cember, Introduction to Health Physics, 3rd ed., McGraw-Hill, 1996.

[49] M. Donya, M. Radford, A. ElGuindy, D. Firmin and M. H. nYacoub, “Radiation in medicine: Origins, risks and aspirations,” *Global Cardilogy Science & Practice,* vol. 204, no. 4, pp. 437 - 448, 2014.

[50] G. Horneck, “Linear Energy Transfer,” in *Encyclopedia of Astrobiology*, Berlin, Springer Heidelberg, 2014.

[51] J. J. Broerse and G. W. Barendsen, “The Physics of Absorbed Dose and Linear Energy Transfer,” in *Radiation Carcinogenesis and DNA Alterations,* Boston MA, Springer, , 1986, pp. 593- 609.

[52] D. Omar, D. Nan and Z. Guangming, “Targeted and non-targeted effects of ionizing radiation,” *Journal of Radiation Research and Applied Sciences,* vol. 8, no. 2, pp. 247- 254, April 2015.

[53] W. M. Dale, “Direct and indirect effects of ionizing radiations,” in *Radiation Biology*, vol. 2, A. Zuppinger, Ed., Berlin, Heidelberg, Springer, 1966, pp. 1-38.

[54] A. H. Elgazzar, “Biological Effects of Ionizing Radiation,” in *The Pathophysiologic Basis of Nuclear Medicine*, Berlin, Heidelberg, Springer, 2006, pp. 540 - 548.

[55] B. E. Norman, “Basic Review of Radiation Biology and Terminology,” *Journal of Nuclear Medicine and Terminology* , vol. 29, no. 2, pp. 67 - 73, 2001.

[56] C. W. Mays, “Stochastic and non-stochastic concepts: Is revision needed?,” *Health Physics,* vol. 55, no. 2, pp. 437 - 441, 1988.

[57] A. C. Upton, “Cancer induction and non-stochastic effects,” *The British Journal of Radiology,* vol. 60, no. 709, pp. 1- 16, 1987.

[58] A. Masitah, H. Zaini, S. Ahmad, O. Mohamat and K. W. Abdul, “An assesment of absorbed dose and radiation hazard index from natural radioactivity,” *The Malaysian Journal Of Analytical Sciences,* vol. 12, no. 1, 2008.

[59] United Nations Scientic Committee on the effects of atomic Radiation (UNSCEAR), “Radiation Effects and Sources,” United Nations Environmental Programme, 2016.

[60] H. H. Berry, C. J. Rocher, M. Paxton and T. Cooper, “Origin and meaning of place names in Etosha National Park, Namibia,” *Madoqua,* vol. 20, no. 1, pp. 13 - 35, 1997.

[61] Namibia Statistics Agency (NSA), “Namibia Population and Housing census,” 2011.

[62] G. Karahan and A. Bayulken, “Assessment of gamma dose rates around Istanbul (Turkey),” *Journal of Environmental Radioactivity,* vol. 47, no. 2000, pp. 213-221, 2000.

[63] M. Alamgir, K. Masud and M. Rahmatullal, “Natural Radioactivity and Associated Dose Rates in Soil Samples of Malnichera Tea Garden in Sylhet District of Bangladesh,” *Journal of Nuclear and Particle Physics* , vol. 2, no. 6, pp. 147 - 152, 2012.

[64] A. S. Rash, M. S. Raghad and O. O. Rana, “The Activity Concentrations and Radium Equivalent Activity in Soil Samples Collected from the Eastern Part of Basrah Governorate in Southern Iraq,” *International Journal of Analytical Chemistry,* p. 11, 2018.

[65] I. F. Al-Hamarneh and M. I. Awadallah, “Soil Radioactivity Levels and Radiation Hazard Assessment in the Highlands of Northern Jordan,” *Radiation Measurements,* vol. 44, pp. 102-110, 2009.

[66] S. Turhan, U. N. Baykan and K. Sen, “Measurement of the natural radioactivity in building materials used in Ankara and assessment of external doses,” *Journal of Radiological protection,* vol. 28, pp. 83-91, 2008.

[67] W. Isabel and N. Peter, “Summarising bivariate data: regression and correlation analysis,” in *Statistical methods and calculation skills,* Cape Town, Lan Sdowne, 2015, pp. 114-119.

**APPENDIX I**

**Activity Concentrations of $^{238}U$, $^{232}Th$ and $^{40}K$ in the soil samples collected across Outjo. (σ is the error on the concentrations)**

| Sample | Area | Radionuclide concentrations (Bq $kg^{-1}$) | | | | | |
|---|---|---|---|---|---|---|---|
| | | $^{238}U$ | σ | $^{232}Th$ | σ | $^{40}K$ | σ |
| 1 | EP1 | 15.2 | 1.6 | 20.2 | 2.5 | 269.8 | 14.5 |
| 2 | EP2 | 25.8 | 2.0 | 41.0 | 3.5 | 348.7 | 17.4 |
| 3 | EP3 | 23.2 | 2,1 | 42.5 | 3.6 | 352.3 | 17.3 |
| 4 | EP4 | 19.7 | 1.6 | 35.2 | 3.3 | 341.1 | 17.1 |
| 5 | EP5 | 22.4 | 1.8 | 39.6 | 3.3 | 322,3 | 16.7 |
| 6 | JS1 | 28.4 | 1.9 | 35.2 | 3.2 | 385.4 | 18.5 |
| 7 | JS2 | 20.7 | 1.7 | 31.3 | 3.6 | 340.6 | 16.9 |
| 8 | JS3 | 21.9 | 1.8 | 22.5 | 1.8 | 243.3 | 13.8 |
| 9 | JS4 | 25.0 | 2.1 | 35.2 | 3.1 | 289.2 | 15.4 |
| 10 | JS5 | 25.6 | 1.8 | 28.2 | 3.2 | 314.1 | 16.4 |
| 11 | UA1 | 21.5 | 1.9 | 33.6 | 3.5 | 289.2 | 16.9 |
| 12 | UA2 | 19.5 | 1.8 | 31.3 | 3.3 | 342.1 | 13.8 |
| 13 | UA3 | 21.4 | 1.8 | 39.8 | 3.2 | 387.9 | 18.8 |
| 14 | UA4 | 19.6 | 1.7 | 34.9 | 3.1 | 298.3 | 15.6 |
| 15 | UA5 | 20.5 | 1.9 | 32.5 | 3.4 | 298.8 | 15.5 |
| 16 | RI1 | 19.3 | 1.7 | 22.0 | 2.8 | 240.3 | 13.6 |
| 17 | RI2 | 22.0 | 1.7 | 25.1 | 2.8 | 266.3 | 14.6 |
| 18 | RI3 | 15.9 | 1.7 | 23.5 | 2.7 | 246.4 | 13.9 |

| | | | | | | | |
|---|---|---|---|---|---|---|---|
| 19 | RI4 | 19.1 | 1.8 | 26.7 | 2.9 | 271.3 | 14.5 |
| 20 | RI5 | 18.6 | 1.6 | 21.4 | 2.7 | 240.8 | 13.8 |
| 21 | HA1 | 17.9 | 1.8 | 30.1 | 3.0 | 310.0 | 16.1 |
| 22 | HA2 | 20.2 | 1.8 | 29.5 | 2.7 | 252.0 | 14.7 |
| 23 | HA3 | 16.3 | 1.6 | 29.8 | 2.9 | 216.4 | 13.0 |
| 24 | HA4 | 11.7 | 1.6 | 19.9 | 2.7 | 260.7 | 14.3 |
| 25 | HA5 | 19.2 | 1.8 | 34.9 | 3.4 | 411.9 | 19.5 |
| 26 | OM1 | 20.6 | 1.7 | 32.0 | 3.2 | 524.4 | 23.0 |
| 27 | OM2 | 18.6 | 1.7 | 23.4 | 2.8 | 206.2 | 12.9 |
| 28 | OM3 | 15.9 | 1.4 | 23.8 | 2.9 | 279.0 | 15.5 |
| 29 | OM4 | 20.6 | 2.0 | 43.6 | 3.6 | 427.1 | 19.9 |
| 30 | OM5 | 17.5 | 1.5 | 19.7 | 2.6 | 319.2 | 16.4 |
| 31 | OT1 | 22.1 | 1.9 | 36.4 | 3.3 | 397.6 | 19.1 |
| 32 | OT2 | 17.5 | 1.6 | 34.2 | 3.2 | 490.3 | 21.7 |
| 33 | OT3 | 24.3 | 1.8 | 34.2 | 3.1 | 364.0 | 17.7 |
| 34 | OT4 | 26.5 | 1.8 | 37.1 | 3.2 | 378.8 | 18.7 |
| 35 | OT5 | 20.2 | 1.8 | 25.8 | 2.9 | 292.7 | 15.7 |
| 36 | MA1 | 16.4 | 1.6 | 29.8 | 2.9 | 298.3 | 15.6 |
| 37 | MA2 | 22.3 | 1.8 | 27.2 | 2.9 | 350.3 | 17.5 |
| 38 | MA3 | 18.5 | 2.0 | 26.9 | 3.4 | 789.1 | 30.9 |
| 39 | MA4 | 17.5 | 1.7 | 23.1 | 2.9 | 308.0 | 16.4 |
| 40 | MA5 | 24.2 | 2.0 | 47.8 | 3.6 | 478.0 | 21.6 |
| 41 | ME1 | 22.0 | 1.8 | 29.5 | 3.2 | 282.5 | 15.1 |
| 42 | ME2 | 17.3 | 1.6 | 15.2 | 1.8 | 251.0 | 13.9 |

| | | | | | | | |
|---|---|---|---|---|---|---|---|
| 43 | ME3 | 18.8 | 1.7 | 20.7 | 2.5 | 281.5 | 15.4 |
| 44 | ME4 | 19.8 | 1.6 | 21.6 | 2.7 | 246.9 | 14.0 |
| 45 | ME5 | 19.5 | 1.7 | 31.6 | 3.1 | 308.5 | 16.0 |
| 46 | OE1 | 22.9 | 1.7 | 42.8 | 3.4 | 524.4 | 23.1 |
| 47 | OE2 | 29.8 | 2.0 | 58.3 | 4.2 | 819.6 | 31.9 |
| 48 | OE3 | 24.0 | 1.7 | 54.8 | 3.9 | 549.8 | 23.8 |
| 49 | OE4 | 20.0 | 1.9 | 29.8 | 3.0 | 452.6 | 20.6 |
| 50 | OE5 | 18.2 | 1.8 | 32.5 | 3.0 | 371.1 | 18.4 |

## APPENDIX II

## PYTHON ANALYSES CODES

```
Python 3.3.3 (v3.3.3:c3896275c0f6, Nov 18 2013, 21:18:40) [MSC
v.1600 32 bit (Intel)] on win32

Type "copyright", "credits" or "license()" for more information.
# program calculates the concentration (Bq/kg) of the nuclides U-
238,Th-232,K-40 in a given sample with net peak area U for U-238, Th
for Th-232 and K for K-40

# it also calculates the Dose rate in nGy/h and the Effective dose
rate in mSv/y

Import math
import numpy as np
f = open ('netpeakareas.txt','r')  #opens the file and reads the
results for U, Th and K Net peak Areas and their errors
contents = f.readlines() # list the contents of the opened file as
strings

# The following code creates an empty list to input net peak areas
of U, U1, Th, Th1, K and K1 in samples
U =[]
U1 =[]
Th =[]
Th1 =[]

K =[]

K1 =[]

for lines in contents:
   spl = lines.strip().split()      #split the lines into columns
   if len(spl)==6:                  # split lines into 6 columns
      a,b,c, d, e, j = lines.split()  # assigns each column to a, b,
c, d, e, f

#The following code appends columns a,b,c,d,e,j into empty lists for
U,Th,K,U1,Th1 and K1
      U.append(float(a))
      Th.append(float(c))
      U1.append(float(b))
```

```
        Th1.append(float(d))
        K.append(float(e))
        K1.append(float(j))
```

**# The following code creates an array of net peak areas U, Th, K and an array of errors on net peak area U1,Th1 and k1**

```
U = np.array(U)
U1 = np.array(U1)
Th = np.array(Th)

Th1 = np.array(Th1)

K = np.array(K)

K1 = np.array(K1)
```

**#the following codes assigns the values of the net peak areas, concentrations and their errors for U-238, Th-232 and K-40 in the standards**

**#it also calculates k for U-238,Th-232 and K-40 in the standards**

```
A_Us = 73200.00

Ae_Us = 302.59

C_Us = 4939.99

Ce_Us = 29.99

k_U = A_Us/C_Us

ke_Us = ((((Ae_Us/A_Us)**2+(Ce_Us/ C_Us)**2)*(k_U)**2)**0.5)

A_Ths = 21400.00

Ae_Ths = 148.75

C_Ths = 3249.99

Ce_Ths = 89.99

k_Th = A_Ths/C_Ths

ke_Ths = ((((Ae_Ths/A_Ths)**2+(Ce_Ths/ C_Ths)**2)*(k_Th)**2)**0.5)

A_Ks = 27500.00

Ae_Ks = 165.81

C_Ks = 14000.00
```

```
Ce_Ks = 400.00

k_K = A_Ks/C_Ks

ke_Ks = ((((Ae_Ks/A_Ks)**2+(Ce_Ks/ C_Ks) **2)*(k_K)**2)**0.5)

For n in U, U1, Th, Th1, K, K1: # this loop calculates the
concentrations and the errors on the concentrations of the
radionuclides in the samples

      U_c = U/k_U

      U_ce = ((((U1/U_c)**2+(ke_Us/k-U)**2)*(U

      -c)**2)***0.5)

      Th_c = Th/k_Th

      Th_ce = ((((Th1/Th_c)**2+(ke_Ths/k-Th)**2)*(Th

      -c)**2)**0.5)

      K_c = K/k_K

      K_ce = ((((K1/U_c)**2+(ke_Ks/k-K)**2)*(K

      -c)**2)***0.5)

for p in U_c, Th_c, K_c, U_ce, Th_ce, K_ce:#calculates the absorbed
dose and their errors

      Dt = 0.042* K_c + 0.429*U_c + 0.666*Th_c

      Dt_er = ((((0.042*K_ce)**2 + (0.429*U_ce)**2 +
(0.666*Th_ce)**2))**0.5)

for q in Dt, Dt_er:  #calculates the effective dose and the errors
on the effective dose

      A_eff_Dose = Dt*0.00876*0.7*0.2

      A_eff_Dose_er = Dt_er*0.00876*0.7*0.2

z = open ('results.txt','w')

z.write ('U_c \t U-ce \t Th_c \t Th_ce \t \t K_c \t \t \t K_ce \t
Dse_rt \t Dse_rt_er \t A_ef_dse \t A_ef_dse_er \n')

i = 0
```

```
for i in range (0,50):

  z.write ('%2.2f \t %2.2f \t \t %2.2f \t \t %2.2f\t \t %2.3f \t \t
%2.2f \t \t %2.2f \t \t %2.2f \t \t %2.3f \t \t %2.3f \n'%(U_c[i],
U_ce[i],Th_c[i],Th_ce[i],   K_c[i],   K_ce[i],   Dt[i],   Dt_er[i],
A_eff_Dose[i], A_eff_Dose_er[i]))

i += 1

f.close()
```